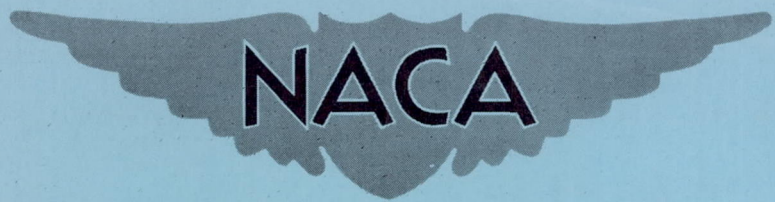CONFIDENTIAL

Copy
RM L52K24

338

P.F.

NACA RM L52K24

NACA

RESEARCH MEMORANDUM

WIND-TUNNEL INVESTIGATION TO DETERMINE THE AERODYNAMIC

CHARACTERISTICS IN STEADY ROLL OF A MODEL

AT HIGH SUBSONIC SPEEDS

By Richard E. Kuhn and James W. Wiggins

Langley Aeronautical Laboratory
Langley Field, Va.

CLASSIFICATION CHANGED TO UNCLASSIFIED
AUTHORITY: NASA PUBLICATION ANNOUNCEMENT NO. 3
EFFECTIVE DATE: DECEMBER 3, 1958
WHL

CLASSIFIED DOCUMENT

This material contains information affecting the National Defense of the United States within the meaning
of the espionage laws, Title 18, U.S.C., Secs. 793 and 794, the transmission or revelation of which in any
manner to an unauthorized person is prohibited by law.

NATIONAL ADVISORY COMMITTEE
FOR AERONAUTICS
WASHINGTON
January 21, 1953

v3

CONFIDENTIAL

NATIONAL ADVISORY COMMITTEE FOR AERONAUTICS

———————

RESEARCH MEMORANDUM

———————

WIND-TUNNEL INVESTIGATION TO DETERMINE THE AERODYNAMIC

CHARACTERISTICS IN STEADY ROLL OF A MODEL

AT HIGH SUBSONIC SPEEDS

By Richard E. Kuhn and James W. Wiggins

SUMMARY

Aerodynamic characteristics in steady roll were obtained in the Langley high-speed 7- by 10-foot tunnel on a complete model and its component parts. The wing and horizontal tail were swept back 45° at the quarter-chord line and had a taper ratio of 0.6, an aspect ratio of 4, and NACA 65A006 airfoil sections parallel to the plane of symmetry. The vertical tail was swept back 55° at the quarter-chord line, had a taper ratio of 0.5, an aspect ratio of 1.2, and an NACA $63_{(10)}A009$ airfoil section parallel to the fuselage center line. The investigation covered a Mach number-range from 0.40 to 0.95 and an angle-of-attack range from 0° to 6°.

In general, the effects of Mach number were small and the over-all comparison of theory with the experimental rolling derivatives at Mach numbers below the force break was not greatly different from that which has been established at low speeds. The theoretical variation of the damping-in-roll parameter C_{l_p} with Mach number at zero lift was in very good agreement with experiment, although the predicted variation with angle of attack and lift coefficient was only fair. The theoretical variation of the slope of the curve of yawing moment due to rolling against lift coefficient C_{n_p}/C_L with Mach number was in good agreement with experiment up to the force-break Mach number, above which an abrupt reduction in C_{n_p}/C_L occurred. The predicted variation of the coefficient of yawing moment due to rolling C_{n_p} with lift coefficient was in excellent agreement with the experimental data. Theoretical predictions of the coefficient of lateral force due to rolling C_{Y_p} were in poor agreement with experiment. The theoretical estimation of the effect of the rolling flow induced by the wing on the vertical-tail contribution to C_{n_p} was good, although somewhat too small particularly at the higher Mach numbers.

INTRODUCTION

A general research program is being carried out in the Langley high-speed 7- by 10-foot tunnel to determine the aerodynamic characteristics in pitch, sideslip, and steady roll of various model configurations. This paper presents data obtained during steady-roll tests of a complete swept-wing model and its component parts. The wing and horizontal tail of the model were swept back 45° at the quarter-chord lines and the vertical tail was swept back 55° at the quarter-chord line. The sting-mounted model was tested through a Mach number range from 0.40 to approximately 0.95 which gave a mean test Reynolds number range based on the mean aerodynamic chord of the wing from about 1.8×10^6 to approximately 3.0×10^6.

Static longitudinal stability characteristics for the wing-fuselage combination of the present model are presented in reference 1.

COEFFICIENTS AND SYMBOLS

The symbols used in the present paper are defined in the following list. All forces and moments are referred to the stability axes (fig. 1), with the origin at the quarter-chord point of the wing mean aerodynamic chord.

C_L lift coefficient, Lift/qS

C_D drag coefficient, Drag/qS

C_l rolling-moment coefficient, Rolling moment/qSb

C_Y lateral-force coefficient, Lateral force/qS

C_n yawing-moment coefficient, Yawing moment/qSb

a speed of sound, ft/sec

V free-stream velocity, ft/sec

M free-stream Mach number, V/a

ρ air density, slugs/cu ft

q dynamic pressure, $\rho V^2/2$, lb/sq ft

b   wing span, ft

S   wing area, sq ft

c   local wing chord, ft

$\bar{c}$ wing mean aerodynamic chord, $\quad 2/S \int_0^{b/2} c^2 dy$, ft

R   Reynolds number based on $\bar{c}$

α angle of attack of wing, deg

$\Delta\alpha$ local angle-of-attack change due to aeroelastic distortion of
            wing, radians

β angle of sideslip, deg

p   rolling angular velocity, radians/sec

$\dfrac{pb}{2V}$ wing-tip helix angle, radians

K   correction factor for aeroelastic distortion

A   aspect ratio, b^2/S

t/c   thickness ratio

l_V tail length; distance, measured parallel to fuselage center
            line, from moment reference point to center of pressure of
            vertical tail, ft

z_V tail height; distance, measured normal to fuselage center line,
            from moment reference point to center of pressure of vertical
            tail, ft

$C_{Y_p} = \dfrac{\partial C_Y}{\partial \frac{pb}{2V}}$

$C_{n_p} = \dfrac{\partial C_n}{\partial \frac{pb}{2V}}$

$C_{l_p} = \dfrac{\partial C_l}{\partial \frac{pb}{2V}}$

Subscripts and abbreviations:

W   wing

F   fuselage

V   vertical tail

H   horizontal tail

m   measured values

L   static loading

MODEL AND APPARATUS

A three-view drawing of the test model and a tabulation of its geometric characteristics are shown in figure 2. The wing and horizontal tail had an NACA 65A006 airfoil section parallel to the plane of symmetry. The wing panels were of a composite construction, consisting of a steel insert with a bismuth-tin covering to give the section contour. The tail section and fuselage were constructed of aluminum alloy. A photograph of the model on the forced-roll sting-support system is shown in figure 3. Figure 4 shows a view of the complete support system used for the forced-roll tests. A schematic view of the forced-roll drive system is shown in figure 5. The model was rotated about the x-axis of the stability axes system. The angle of attack was changed by the use of offset sting adapters as shown in figures 3 and 5. The model was driven by a constant-displacement reversible hydraulic motor, located inside the main sting body, which was actuated by a variable-displacement hydraulic pump driven by a constant-speed electric motor.

The rotational speed was measured by a calibrated microammeter that was connected to a gear-driven direct-current generator mounted inside the main sting body. Speed of rotation was varied by controlling the fluid displacement of the hydraulic pump, and the direction of rotation was changed by reversing the fluid flow through an arrangement of electrically controlled solenoid valves in the hydraulic system.

The forces and moments, measured by an electrical strain-gage balance incorporated inside the model, were transmitted to the recording devices through an arrangement of brushes and slip rings.

TESTS AND CORRECTIONS

The forced-roll tests were conducted in the Langley high-speed 7-by 10-foot tunnel through a Mach number range from approximately 0.40 to 0.95, and through an angle-of-attack range from 0° to 6°. The wing-tip helix-angle (pb/2V) range, corresponding to a revolutions-per-minute range from -150 to 450, is presented in figure 6.

The blocking corrections which were applied to the dynamic pressure and Mach number were determined by the method of reference 2. The size of the model caused the tunnel to choke at a corrected Mach number of about 0.96. An investigation of the jet-boundary corrections to the rotary derivatives by the method of reference 3 indicated that these corrections are negligible. Jet-boundary corrections applied to the lift were calculated by the method of reference 4. There were no tare corrections available to apply to these data; however, the static tare tests conducted in connection with an unpublished investigation of the static lateral stability characteristics of this model indicate the effect of the sting support to be very small.

The support system deflected under load and these deflections, combined with any initial displacement of the mass center of gravity of the model from the roll axis, introduced centrifugal forces and moments when the model was rotated. Corrections for these forces and moments were determined and have been applied to these data.

The wing was known to deflect under load. When the model was forced to roll, the opposing rolling moment distorted the wing in such a manner as to reduce the angle of attack on the down-going wing and increase the angle of attack on the up-going wing. Accordingly, in an effort to correct the measured data to correspond to the rigid case, a correction factor for the effect of this aeroelastic distortion on the rolling moment was determined with the aid of static loadings. The theoretical spanwise load distribution due to roll of reference 5 was simulated by loading the wing at four spanwise points on the quarter-chord line. The change in angle of attack $\Delta\alpha$ (fig. 7(a)) was measured by dial gages at several spanwise stations in the chordwise plane parallel to the plane of symmetry. An equivalent linear variation of $\Delta\alpha$ (fig. 7(a)) was determined which corresponds to the angle-of-attack distribution produced

by an increment of wing-tip helix angle $\Delta\left(\dfrac{pb}{2V}\right)$. The corrected damping-in-roll coefficient can be written in terms of the measured values and this increment as follows

$$C_{l_p} = \frac{C_{l_m}}{\left(\dfrac{pb}{2V}\right)_m - \Delta\left(\dfrac{pb}{2V}\right)} = \frac{\left(C_{l_p}\right)_m}{1 - KC_{l_{p_m}}}$$

where

$$K = \frac{\Delta\left(\frac{pb}{2V}\right)}{C_{l_m}} = \left(\frac{\Delta\alpha}{qC_{l_L}}\right)q$$

where $\Delta\alpha/qC_{l_L}$ is the value at $y = \frac{b}{2}$ (fig. 7(a)). Aeroelastic effects on C_{Y_p} and C_{n_p} were small and therefore neglected.

The angle of attack at the plane of symmetry has been corrected for the deflection of the model and support system under load.

The variation of the mean test Reynolds number with Mach number is presented in figure 8.

RESULTS AND DISCUSSION

Presentation of Results

The results of the investigation are presented in the following figures:

	Figure
Basic data	9 and 10
C_{l_p}	11 to 15
C_{n_p}	16 to 20
C_{Y_p}	21 to 23

The basic data (figs. 9 and 10) have not been corrected for aeroelastic distortion. The rotary derviatives in figure 9 are presented against angle of attack at several Mach numbers; whereas, in figure 10, the derivatives are presented against Mach number at several angles of attack.

A system of designating the various model configurations has been used and is defined as follows:

Complete model	WFVH
Wing, fuselage, and vertical tail	WFV
Wing and fuselage	WF
Fuselage, vertical tail, and horizontal tail	FVH
Fuselage and vertical tail	FV
Fuselage alone	F

Rolling Moment Due to Rolling

Wing-fuselage.- The measured and corrected values of the damping-in-roll derivative C_{l_p} for the wing-fuselage combination at zero angle of attack are presented in figure 11(a), and the corrected values of C_{l_p} are compared with two wing-alone theories in figure 11(b). The theoretical variation of C_{l_p} with Mach number, determined by applying the three-dimensional Prandtl-Glauert plan-form transformation for compressibility effects to the incompressible-flow values of reference 5, is in good agreement with experiment, although the predicted values are somewhat low. The predicted variation of C_{l_p} with Mach number determined by applying the Mach number correction from reference 6 to the incompressible-flow values of reference 5 also is in good agreement with experiment and could probably be used satisfactorily for a general estimation of the effects of compressibility on C_{l_p} since the calculation procedure is somewhat less involved than the Prandtl-Glauert plan-form transformation method.

A comparison of the theoretical wing-alone variation of C_{l_p} with lift coefficient and the corrected wing-fuselage experimental variation is presented in figure 12. Method 3 of reference 7 was applied by using the lift data of reference 1 and by correcting C_{l_p} at zero lift for Mach number effects by the method of reference 6. Near zero lift, the experimental and predicted results are in good agreement at all Mach numbers as previously shown in figure 11; however, the discrepancies apparent at the higher lift coefficients result in part from difficulties in establishing the experimental lift-curve slope at these lift coefficients. The high-speed free-roll data of reference 8 and the low-speed data of reference 7 (wing No. 22) show similar variations.

Tail contributions.- The contributions of the vertical and horizontal tails to C_{l_p} are presented in figures 13 and 14 along with values predicted by the method of reference 9. The experimentally determined tail lift-curve slope and the locations of tail center of pressure used in the theoretical calculations were determined from unpublished static lateral-stability data on the present model; however, calculations using the geometric aspect ratio and tail lengths indicated essentially the same results. The increment of C_{l_p} contributed by the tail surfaces is seen to be small and is adequately predicted.

Complete model.- A comparison of the corrected experimental damping in roll C_{l_p} with predicted values for the complete model at several Mach numbers is presented in figure 15. Since the theory presented is a summation of the theoretical values from figures 12, 13, and 14, and

since the wing contribution to C_{l_p} is predominant, the variation of C_{l_p} for the complete model with angle of attack is quite similar to the wing-fuselage variation presented in figure 12.

Yawing Moment Due to Rolling

Wing-fuselage.- A comparison of the wing-fuselage experimental and the wing-alone theoretical variation of C_{n_p}/C_L with Mach number is presented in figure 16. The experimental points of figure 16 were determined from the slopes of the experimental data between zero and approximately 0.1 lift coefficient. The theory of reference 10 is presented with the first term of equation (4) from reference 10 corrected for the effects of compressibility by the method of reference 6. The experimental data of reference 1 were used for evaluating the profile-drag contribution in accordance with equation (8) of reference 10. The predicted variation with Mach number is in good agreement with the experimental variation, although theory predicts somewhat more negative values. This discrepancy may be largely due to the difficulties of determining the experimental variation of C_{n_p} with lift coefficient because of nonlinearities even at the lowest lift coefficient (fig. 17). An abrupt reduction in the magnitude of C_{n_p}/C_L occurs above the force-break Mach number (fig. 16). This reduction probably results from the drag rise at zero lift and the decrease in the lift-curve slope at the higher Mach numbers (ref. 1) and may possible be augmented by a loss of tip suction.

Figure 17 presents a comparison of the wing-fuselage experimental variation of C_{n_p} with lift coefficient and the wing-alone theoretical variation, where theory includes the effects of both the induced and profile drag (ref. 10). Excellent agreement is indicated at all Mach numbers and lift coefficients.

Tail contributions.- The contribution of the vertical tail to C_{n_p} is presented in figure 18, along with a comparison with theory (ref. 9) for wing-on and wing-off conditions. The tail lengths and tail lift-curve slopes used in the theoretical calculations were determined from unpublished static lateral-stability data on the present model. In general, the agreement is considered good, although theory somewhat underestimates the effect of the rolling flow induced by the wing on the vertical tail, particularly at the higher Mach numbers. This underestimation is also indicated in the data presented in reference 9.

Figure 19(a) shows comparison of tail center-of-pressure locations (given by the length l_V and the height z_V) as determined from static

lateral-stability data and as indicated from simple geometric considerations. These center-of-pressure parameters are applied in calculations of the vertical-tail contribution to C_{n_p} in figure 19(b), and the results are compared with experiment. It is apparent that the predicted variations, using the center of pressure determined from experimental data, are in better agreement with experiment than the predicted variations using the geometric centers of pressure.

Complete model.- A comparison of experimental and theoretical values of C_{n_p} for the complete model at several Mach numbers is shown in figure 20. The theory presented is the sum of the theoretical values from figures 17 and 18. The theoretical C_{n_p} variation with angle of attack is in very good agreement with experiment, although the theoretical values are somewhat more positive, since, as mentioned previously, the theory underestimates the effect of the rolling flow induced by the wing on the vertical tail.

Lateral Force Due to Rolling

Wing-fuselage.- The variation of wing-fuselage experimental and wing-alone theoretical C_{Y_p}/C_L with Mach number is shown in figure 21. The theory of reference 10 is presented with the first term of equation (2) from reference 10 corrected for Mach number effects by the method of reference 6. The term $1/A$ in equation (2) of reference 10 is considered to be independent of Mach number. The predicted values of C_{Y_p}/C_L are in very poor agreement with the experimental values. It should be pointed out, however, that the wing of this investigation has a thin section ($t/c = 0.06$) and an examination of the data of reference 1 indicates that an early increase in the drag increment $\left(C_D - \dfrac{C_L^2}{\pi A}\right)$ would be expected for such a wing. Since the method of reference 10 applies only at lift coefficients below that at which $C_D - \dfrac{C_L^2}{\pi A}$ begins to increase, it appears that the lack of data near zero lift excludes the possibility of measuring a true value of the slope C_{Y_p}/C_L at zero lift coefficient. The low-speed wing-alone data of a thicker wing ($t/c = 0.08$) presented in figure 7 of reference 9 show a substantially higher value of C_{Y_p}/C_L, although the value still is somewhat lower than that predicted by reference 10.

An appreciable reduction in C_{Y_p}/C_L occurred at the higher Mach numbers.

    <u>Tail contribution</u>.- The contribution of the vertical tail to C_{Y_p} with wing on and wing off is presented in figure 22 along with results predicted by means of reference 9. As was indicated in the case of C_{n_p}, the predicted effect of the rolling flow induced by the wing at the tail is too small. The experimental data of reference 9 show similar discrepancies.

    <u>Complete model</u>.- The variation of experimental C_{Y_p} with angle of attack for the complete model is compared with theory in figure 23. The theoretical values presented are the sums of those given in figures 21 and 22. As would be expected from the preceding discussion, theory tends to overestimate the values of C_{Y_p} for the complete model.

<div align="center">CONCLUSIONS</div>

    The results of the investigation to determine the aerodynamic characteristics in steady roll of a complete model and its component parts indicated that, in general, within the range of the tests the effects of Mach number were small and the over-all comparison of theory with experiment at Mach numbers below the force break was not greatly different from that which has been established at low speeds. The following specific conclusions are apparent:

    1. The variation of the damping-in-roll parameter C_{l_p} with Mach number at zero lift is very well predicted by theory; however, the predicted variation with lift coefficient was only in fair agreement with experiment.

    2. The predicted variation of C_{n_p}/C_L (variation of the yawing moment due to rolling with lift coefficient) with Mach number up to the force break and the variation of C_{n_p} with lift coefficient were in in very good agreement with the experimental results. An abrupt reduction in the negative value of C_{n_p}/C_L for the wing-fuselage combination occurred above the force-break Mach number.

    3. The theoretical predictions of the lateral force due to rolling C_{Y_p} were in poor agreement with experiment. A reduction of the positive value of C_{Y_p}/C_L (variation of lateral force due to rolling with lift coefficient) occurred at the higher Mach numbers.

    4. The theoretical estimation of the effect of the rolling flow induced by the wing on the vertical-tail contribution to C_{n_p} and C_{Y_p}

was somewhat smaller than that indicated by experiment, particularly at the higher Mach numbers.

Langley Aeronautical Laboratory,
    National Advisory Committee for Aeronautics,
        Langley Field, Va.

REFERENCES

1. Kuhn, Richard E., and Wiggins, James W.: Wind-Tunnel Investigation of the Aerodynamic Characteristics in Pitch of Wing-Fuselage Combinations at High Subsonic Speeds. Aspect-Ratio Series. NACA RM L52A29, 1952.

2. Hensel, Rudolf W.: Rectangular-Wind-Tunnel Blocking Corrections Using the Velocity-Ratio Method. NACA TN 2372, 1951.

3. Evans, J. M., and Fink, P. T.: Stability Derivatives. Determination of l_p by Free Oscillations. Report ACA-34, Australian Council for Aeronautics, Apr. 1947.

4. Gillis, Clarence L., Polhamus, Edward C., and Gray, Joseph L., Jr.: Charts for Determining Jet-Boundary Corrections for Complete Models in 7- by 10-Foot Closed Rectangular Wind Tunnels. NACA ARR L5G31, 1945.

5. Bird, John D.: Some Theoretical Low-Speed Span Loading Characteristics of Swept Wings in Roll and Sideslip. NACA Rep. 969, 1950. (Supersedes NACA TN 1839.)

6. Fisher, Lewis R.: Approximate Corrections for the Effects of Compressibility on the Subsonic Stability Derivatives of Swept Wings. NACA TN 1854, 1949.

7. Goodman, Alex, and Adair, Glenn H.: Estimation of the Damping in Roll of Wings Through the Normal Flight Range of Lift Coefficient. NACA TN 1924, 1949.

8. Kuhn, Richard E., and Myers, Boyd C., II: Effects of Mach Number and Sweep on the Damping-in-Roll Characteristics of Wings of Aspect Ratio 4. NACA RM L9E10, 1949.

9. Wolhart, Walter D.: Influence of Wing and Fuselage on the Vertical-Tail Contribution to the Low-Speed Rolling Derivatives of Midwing Airplane Models With 45° Sweptback Surfaces. NACA TN 2587, 1951.

10. Goodman, Alex, and Fisher, Lewis R.: Investigation at Low Speeds of the Effect of Aspect Ratio and Sweep on Rolling Stability Derivatives of Untapered Wings. NACA Rep. 968, 1950. (Supersedes NACA TN 1835.)
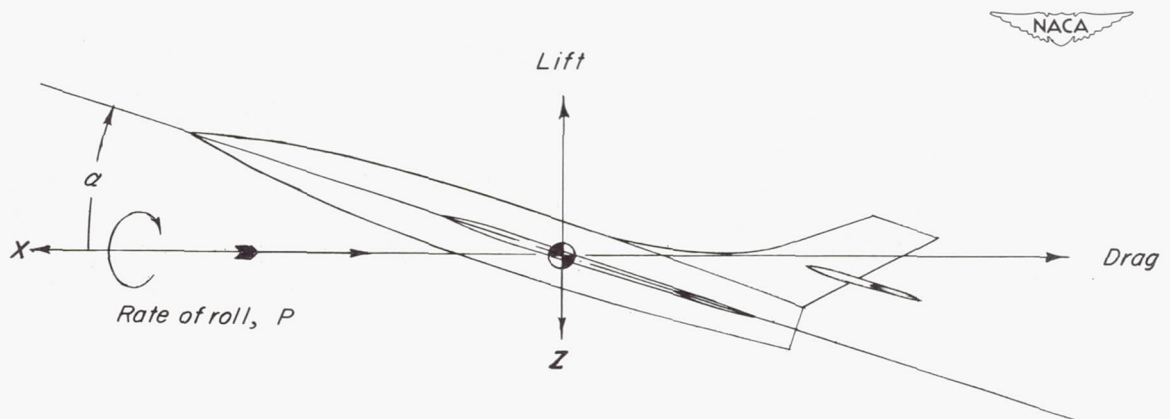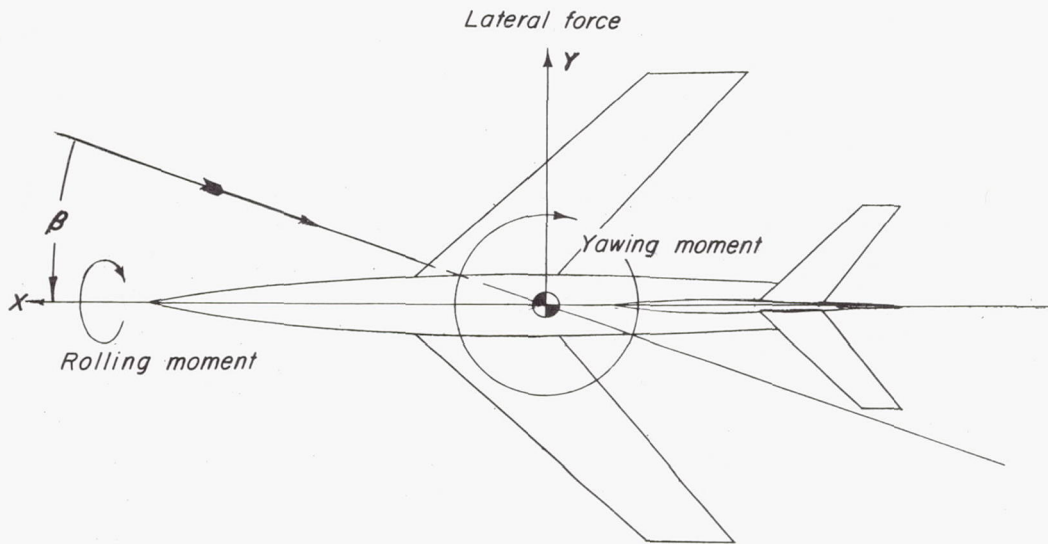
Figure 1.- System of axes used showing the positive direction of forces, moments, angles, and velocities.
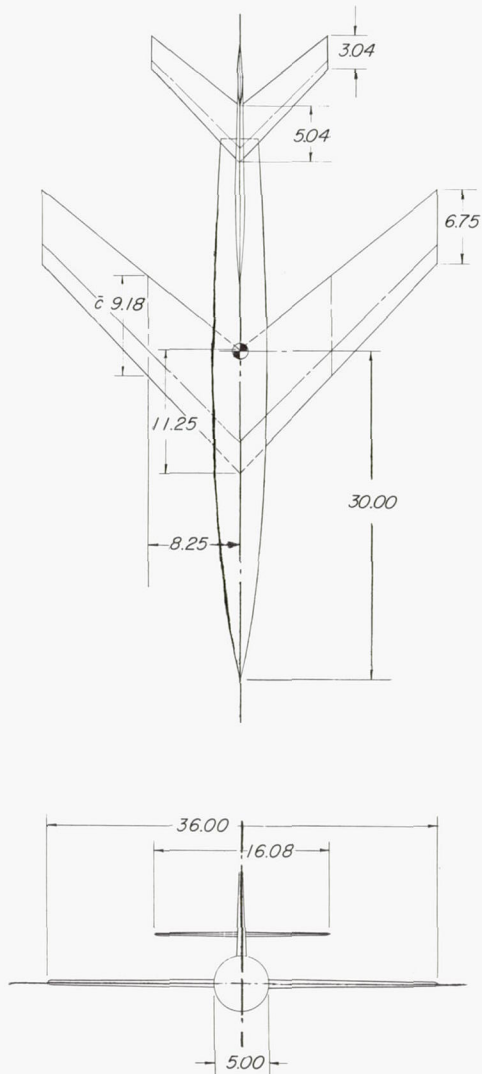
Wing
Area, sq ft ... 2.25
Aspect ratio ... 4
Sweep (a) c/4 ... 45°
Taper ratio 6
Airfoil section streamwise ... 65A006

Horizontal tail
Area, sq ft ... .45
Aspect ratio ... 4
Sweep (a) c/4 ... 45°
Taper ratio 6
Airfoil section streamwise ... 65A006

Vertical tail
Area, sq ft ... .612
Aspect ratio ... 1.177
Sweep (a) T.E. ... 45°
Taper ratio 5
Airfoil section streamwise ... $63_{(10)}$ A009
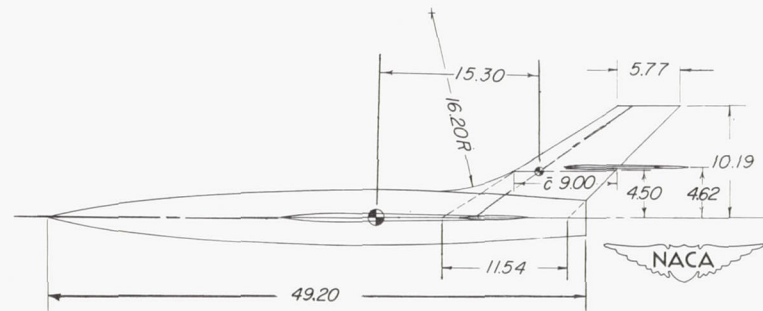
Figure 2.- Three-view drawing of model.
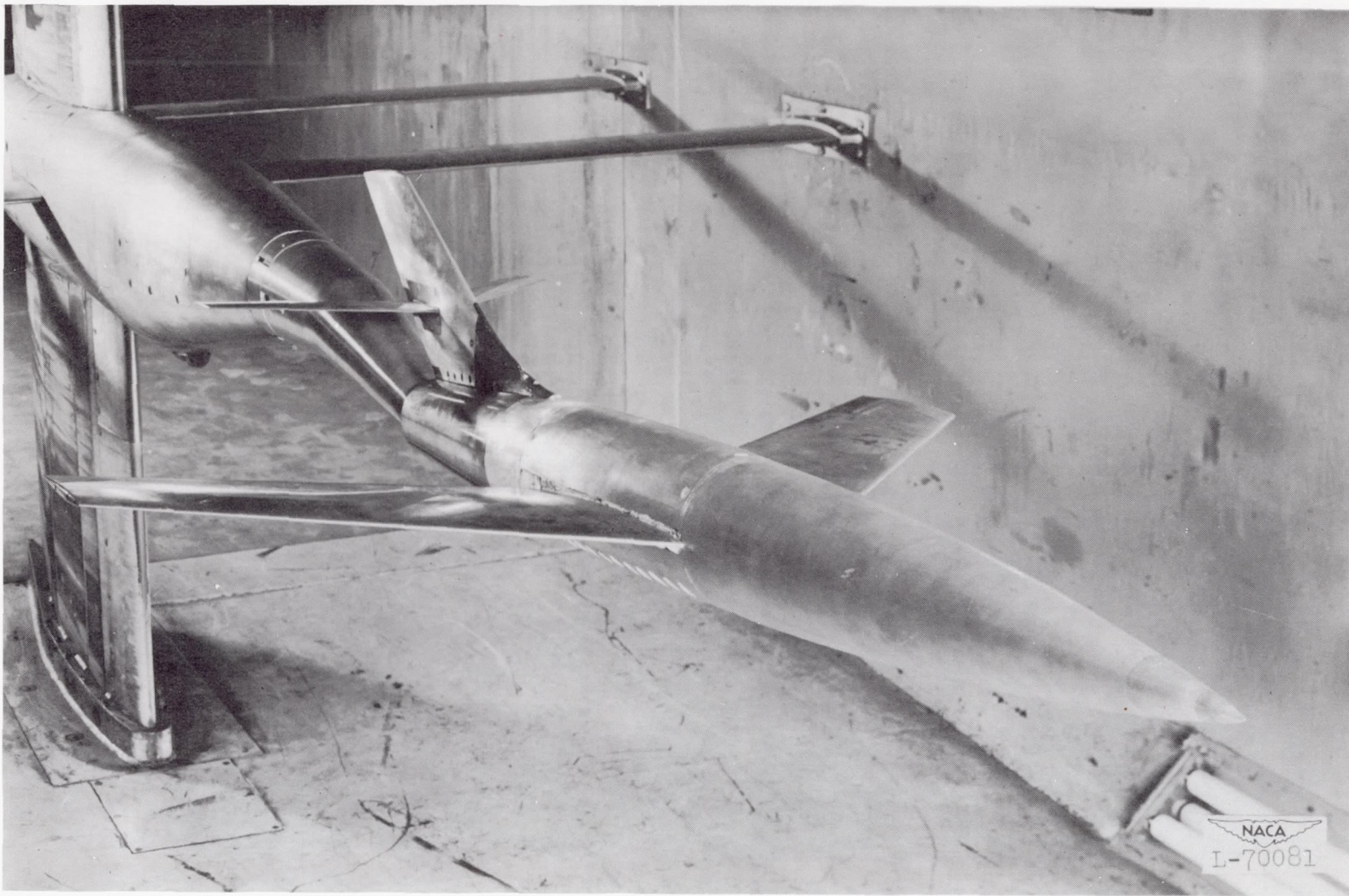
Figure 3.- Photograph of model installed on the forced-roll support system. $\alpha = 6^{\circ}$.
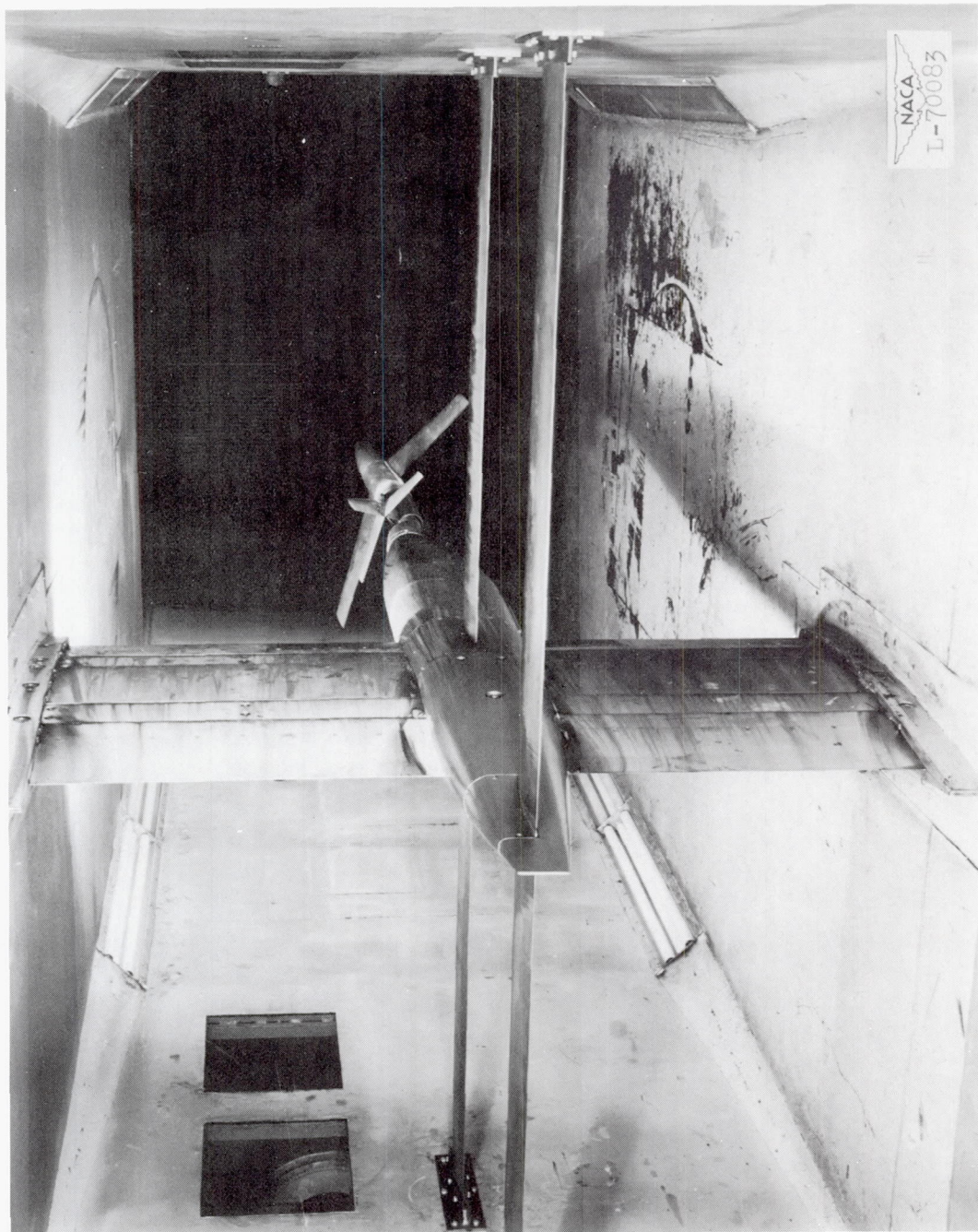
Figure 4.- Rear view of support system and model. $\alpha = 6°$.

TUNNEL CEILING

VERTICAL STRUT

OFFSET STING ADAPTER

OIL SEAL

D.C. GENERATOR FOR TACHOMETER

BRUSHES AND BRUSH HOLDER

LEADS FROM STRAIN-GAGE BALANCE INSIDE THE MODEL

SLIP RINGS

GEAR BOX OIL SUMP

HYDRAULIC MOTOR

TUNNEL FLOOR

NACA

VARIABLE-DISPLACEMENT HYDRAULIC PUMP

25 H.P. ELECTRIC MOTOR
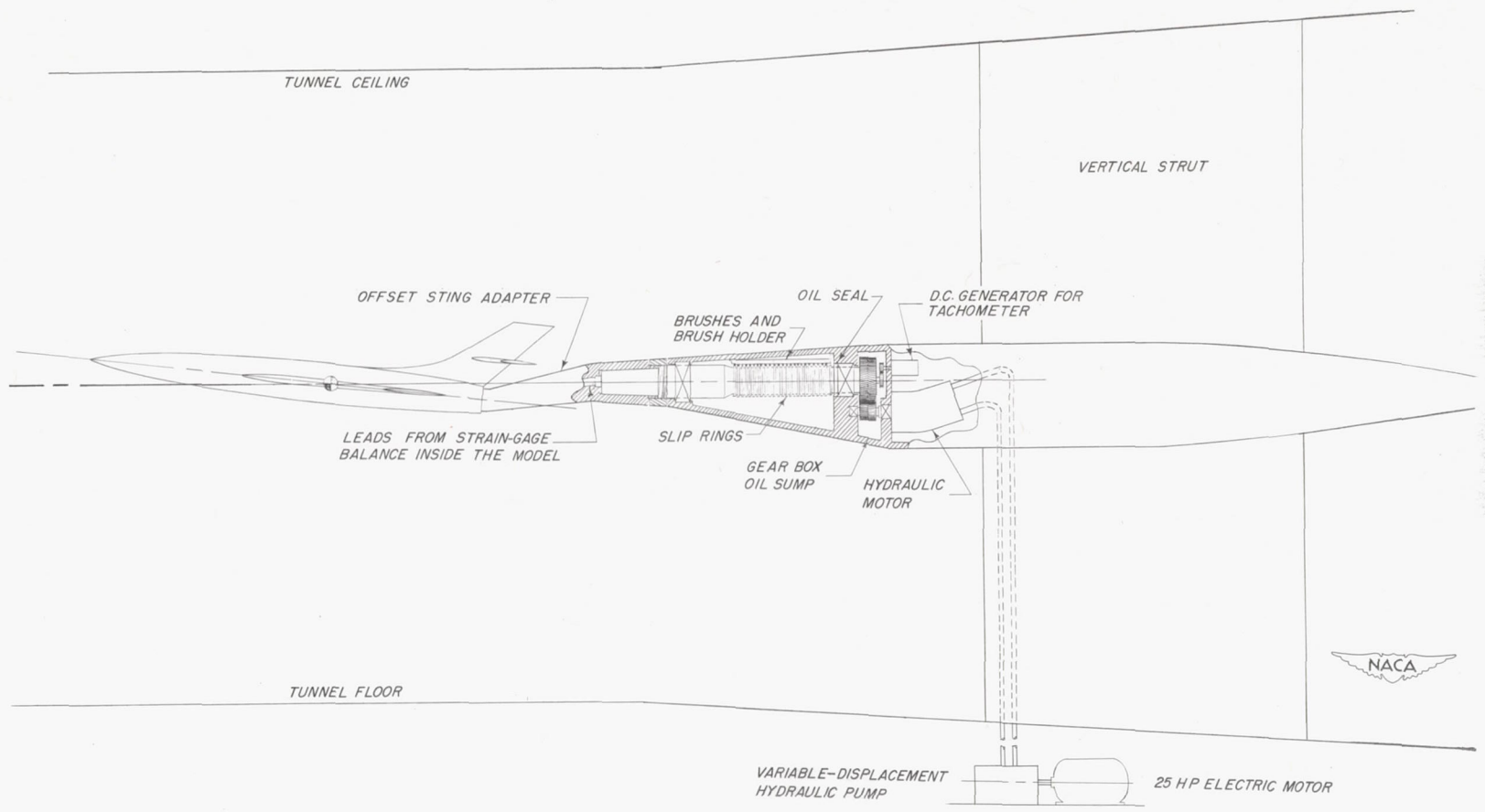
Figure 5.- General arrangement of forced-roll support system.
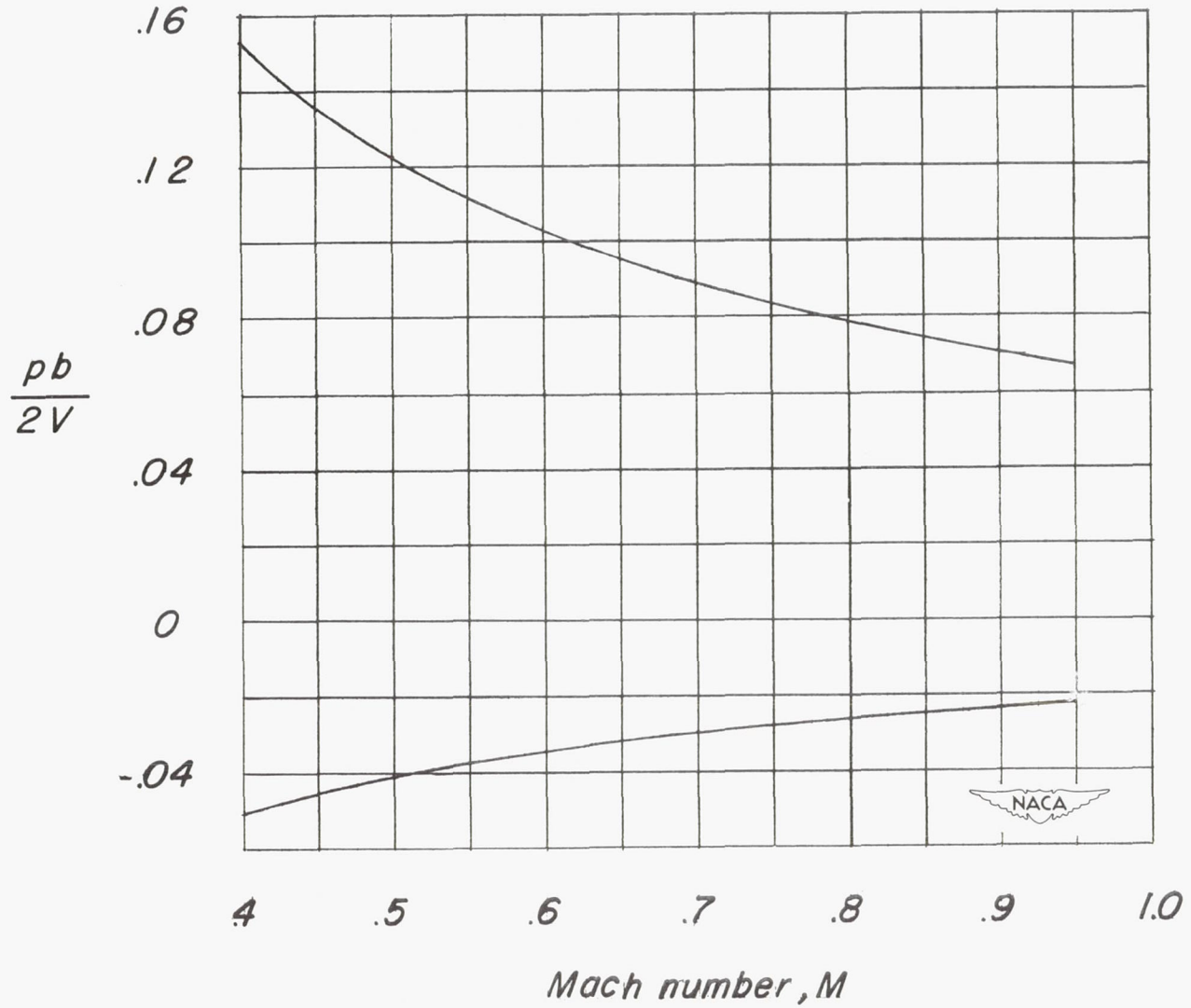
Figure 6.- Limits of the wing-tip helix angle throughout the Mach number range.
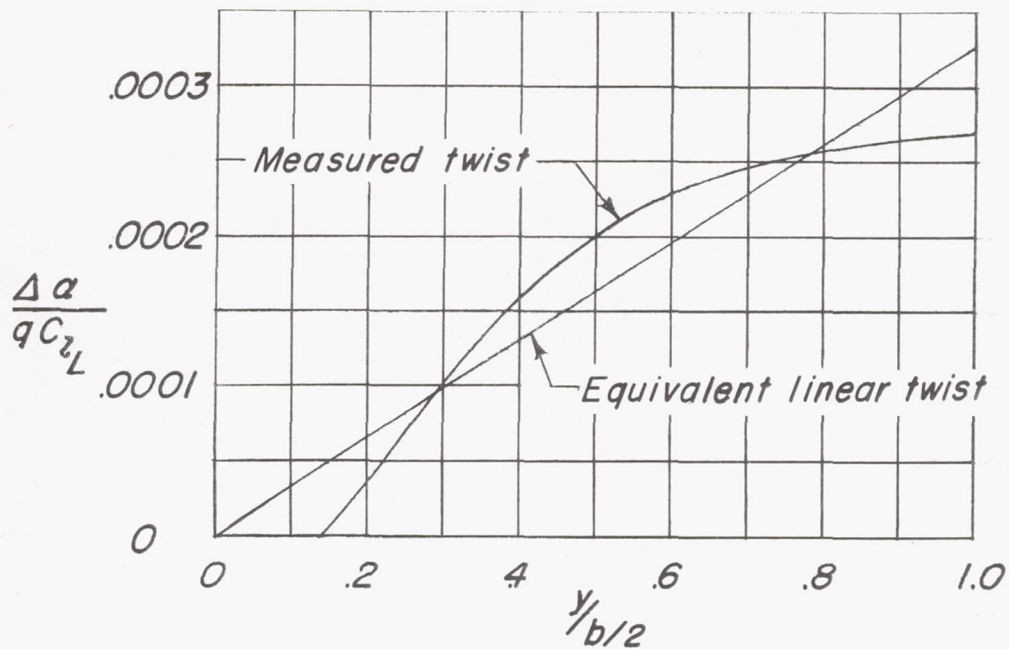
(a) Spanwise distribution of twist caused by
rolling moment due to rolling.
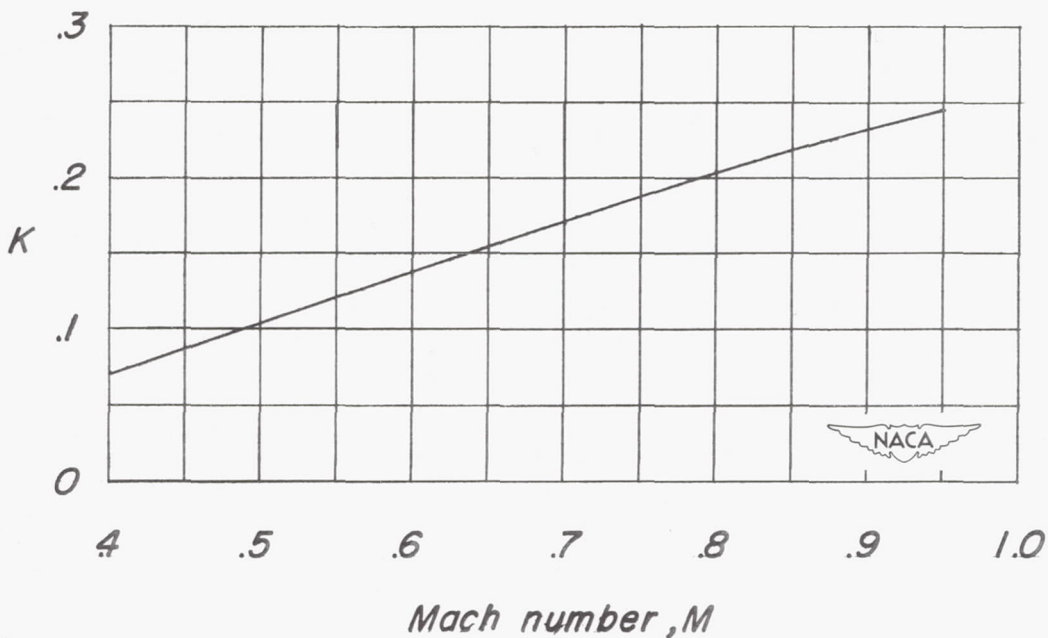
(b) Correction factor for C_{l_p}.

Figure 7.- Aeroelastic characteristics of the wing.
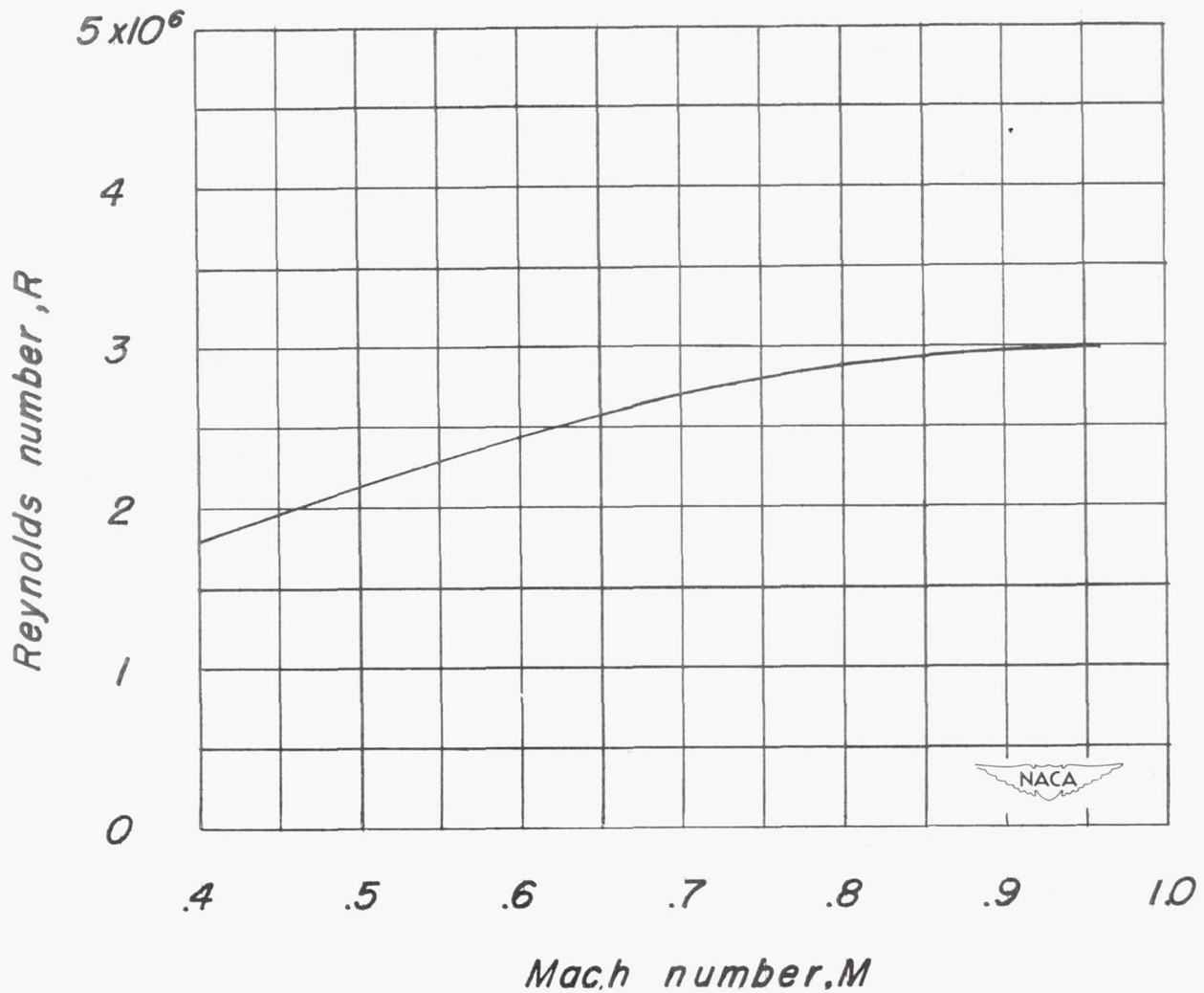
Figure 8.- Variation of the mean test Reynolds number with Mach number based on the mean aerodynamic chord of the wing.
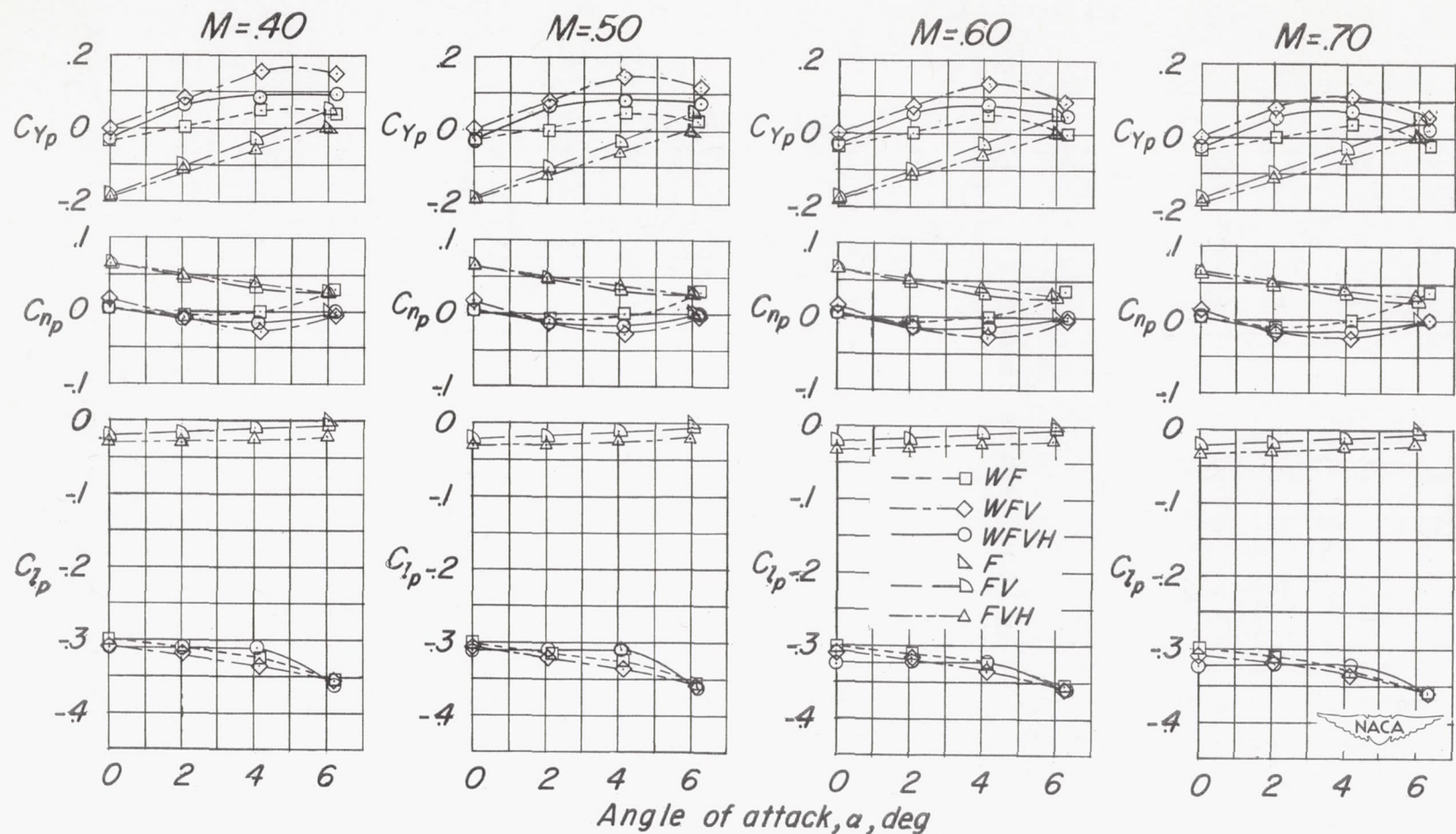
Figure 9.- Variation of the aerodynamic characteristics in roll with angle of attack at several Mach numbers. Data not corrected for aeroelastic distortion.
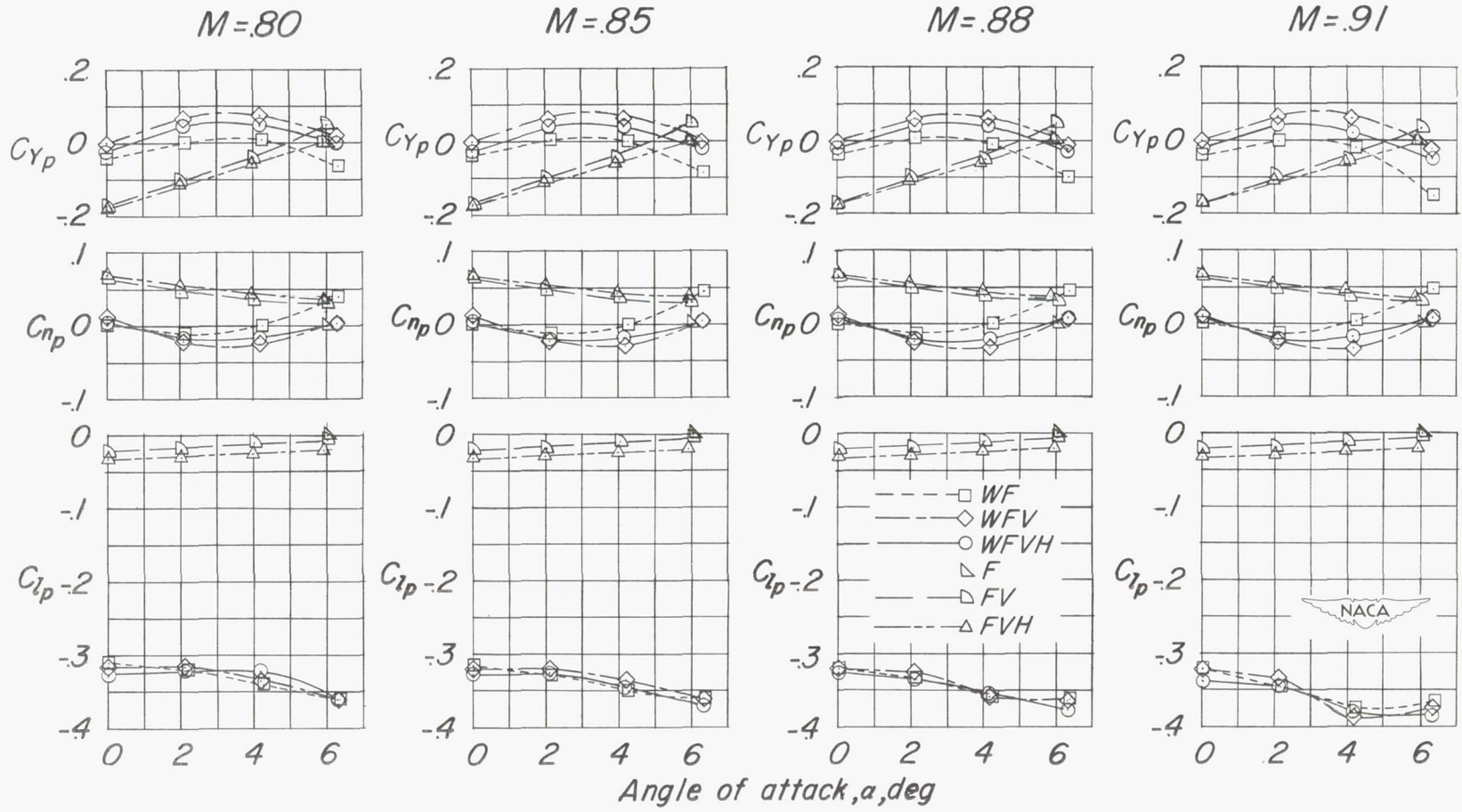
Figure 9.- Continued.
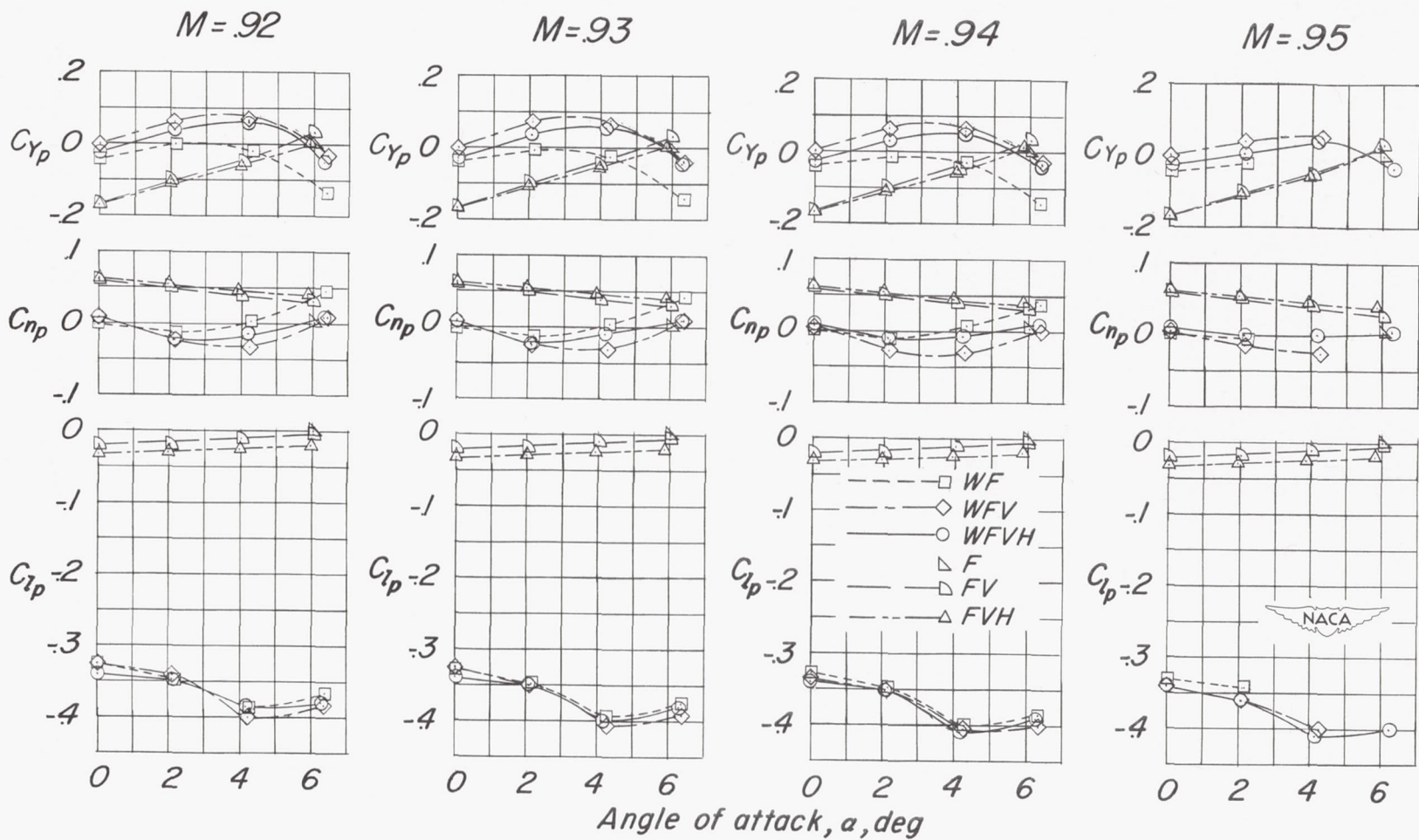
Figure 9.- Concluded.
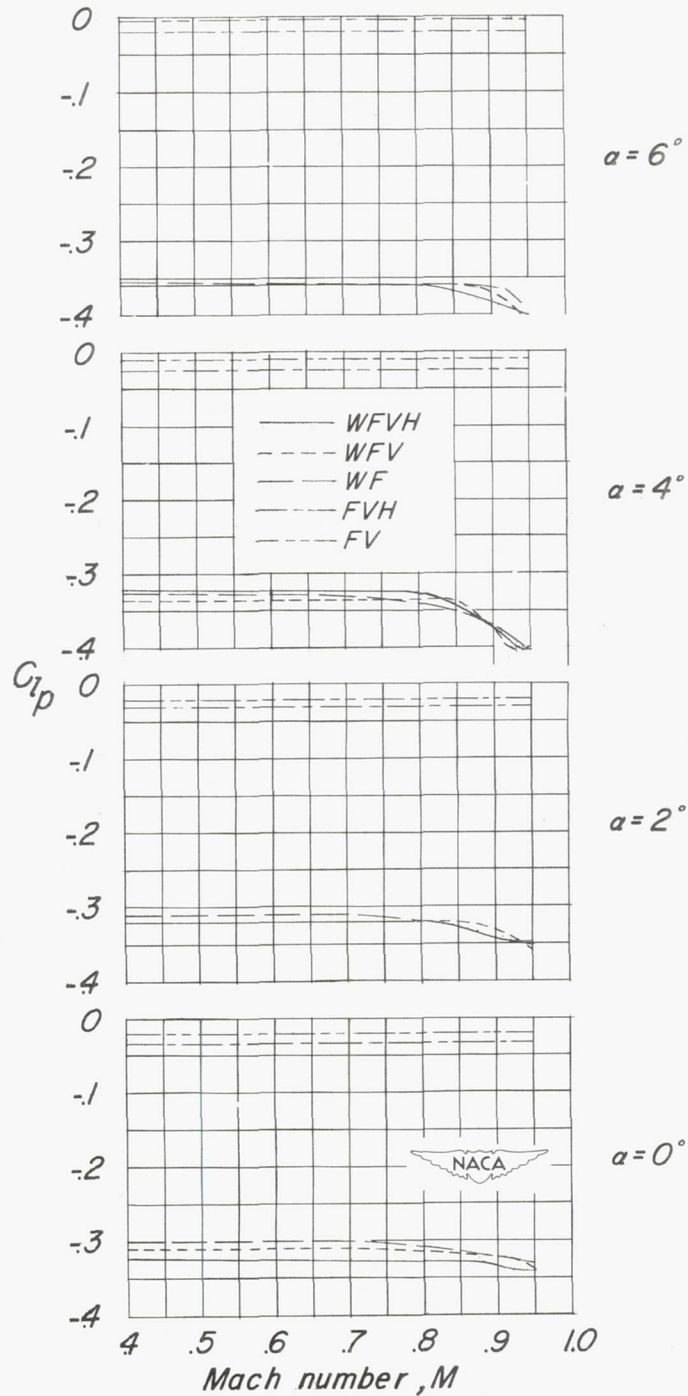
(a) C_{l_p}.

Figure 10.- Variation of the aerodynamic characteristics in roll with
Mach number. Data not corrected for aeroelastic distortion.
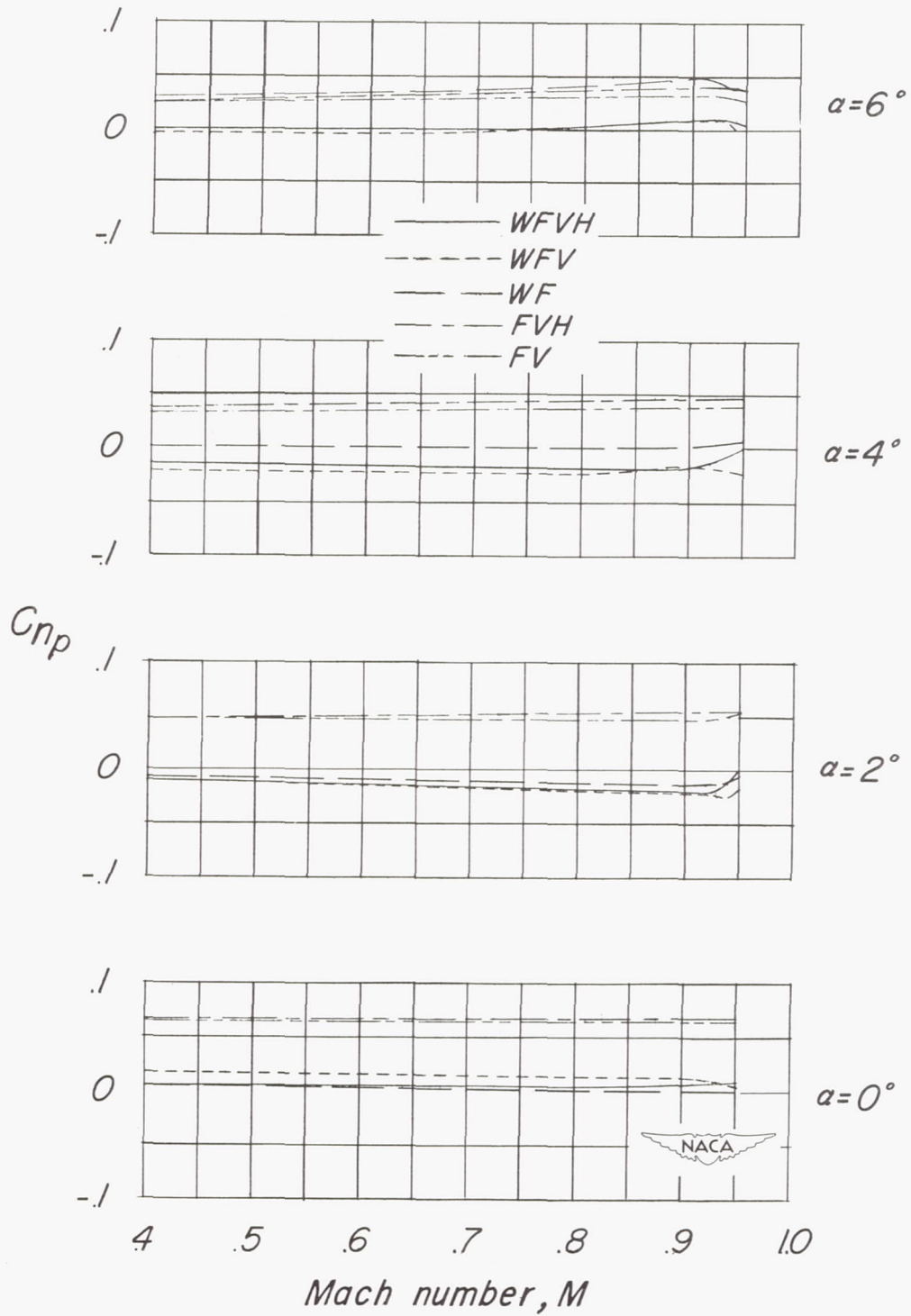
(b) C_{n_p}.

Figure 10.- Continued.
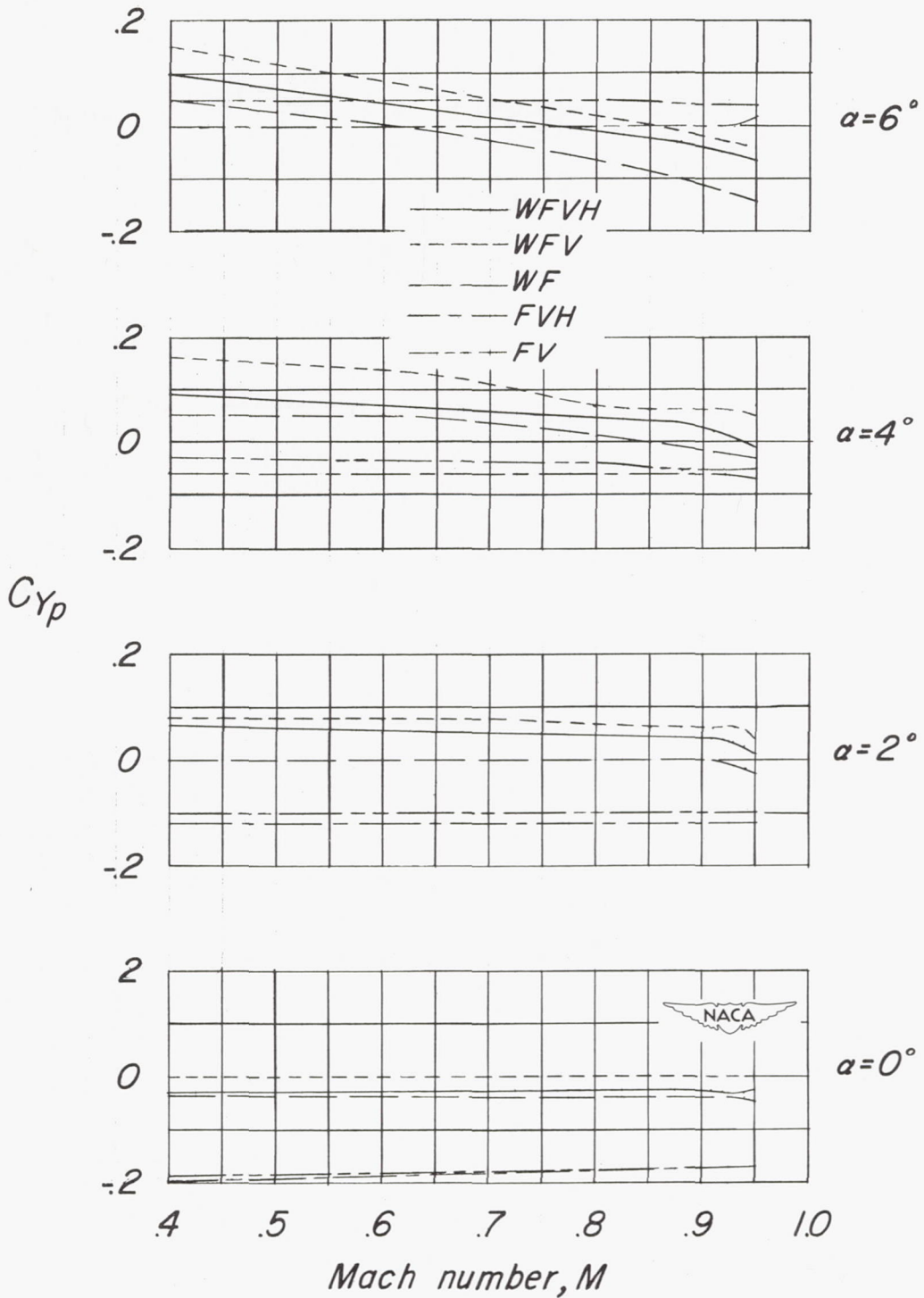
(c) C_{Y_p}.

Figure 10.- Concluded.
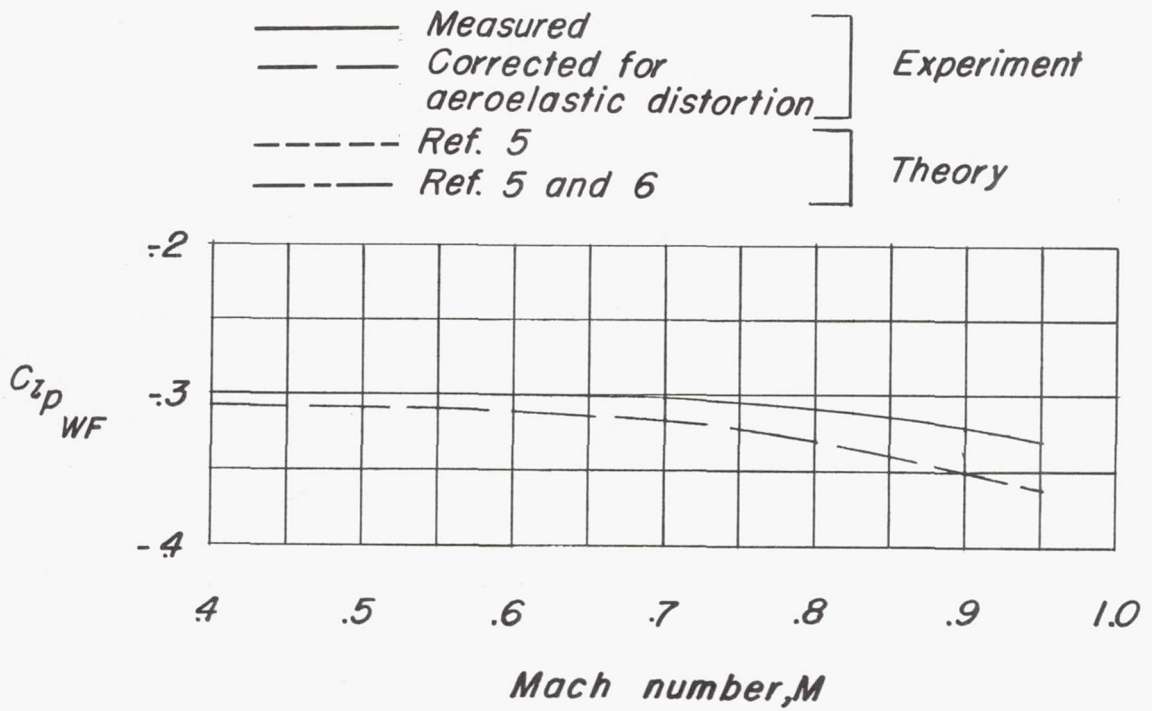
(a) Effects of aeroelasticity on C_{l_p}.
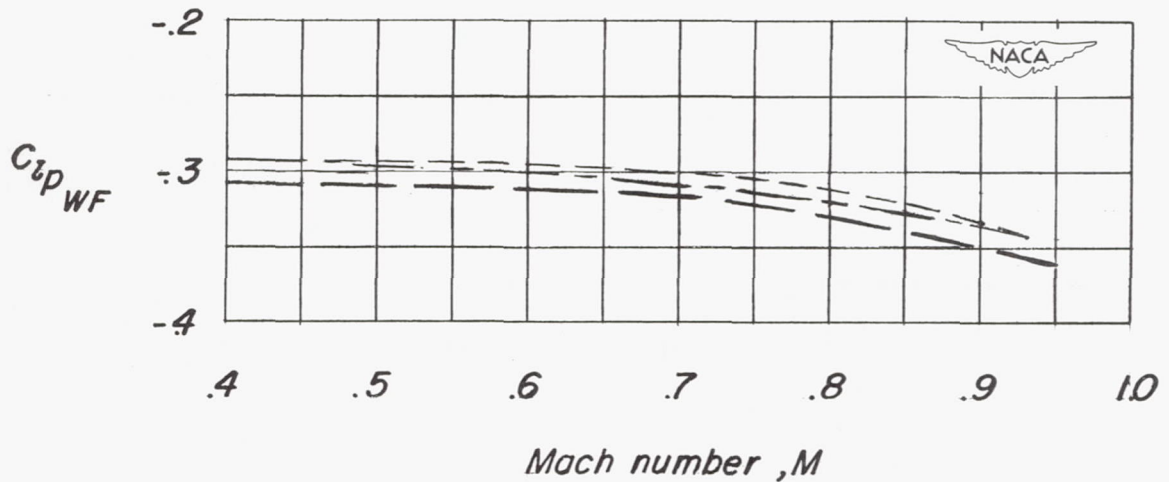
(b) Comparison of experimental and theoretical values of C_{l_p}.

Figure 11.- Effects of aeroelastic distortion and Mach number on damping in roll of the wing-fuselage combination. $\alpha = 0^{\circ}$.

○ Experimental data
(corrected for aeroelastic distortion)

— — Wing-alone theory (ref. 6 and 7)
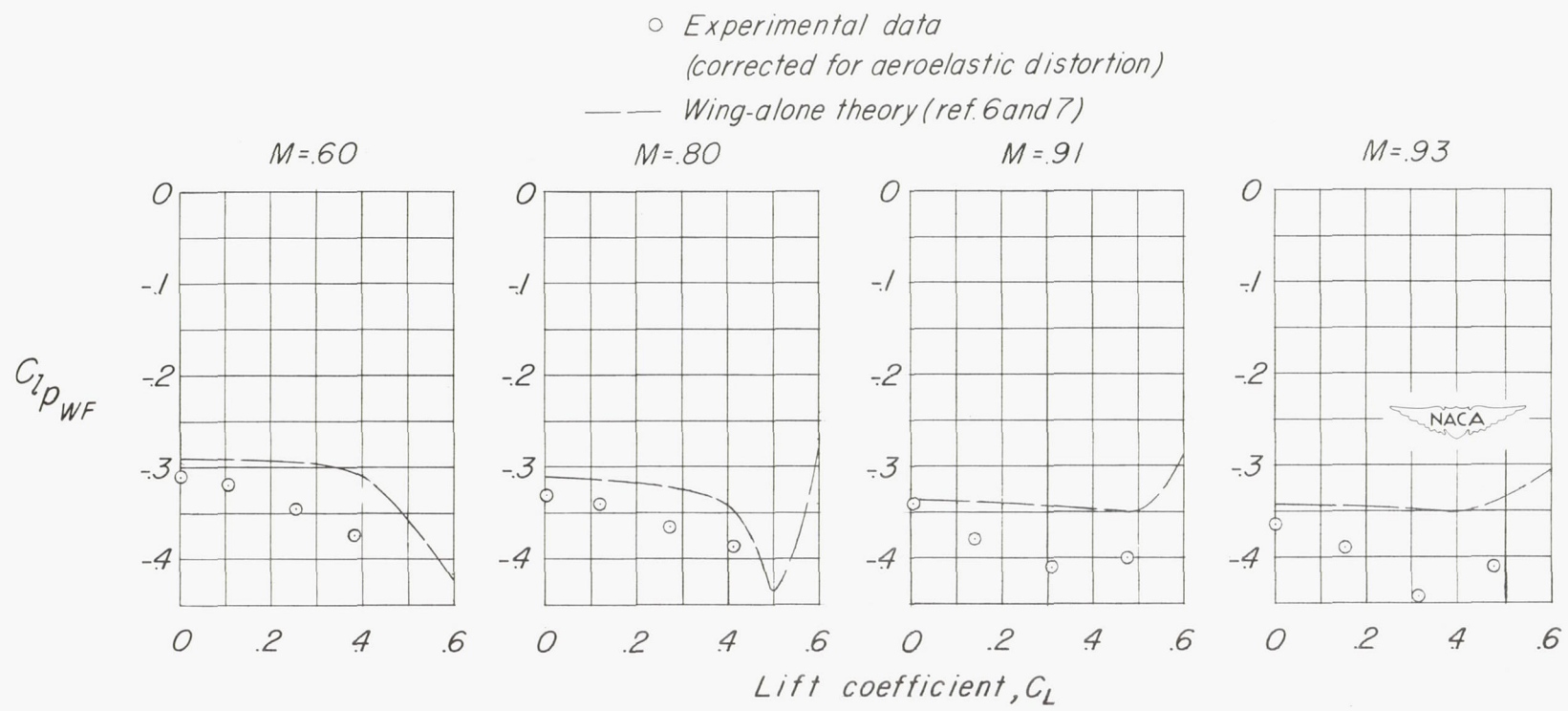
Figure 12.- Comparison of the experimental wing-fuselage C_{l_p} and theoretical wing-alone C_{l_p} at several Mach numbers.

Wing off (FV-F)   Experiment   Theory

Wing on (WFV-WF)   ∘   ⎤
                                      ⎦ Ref. 9

$C_{l_{p_V}}$

M = .93

M = .91

M = .80

M = .60

Angle of attack, α, deg
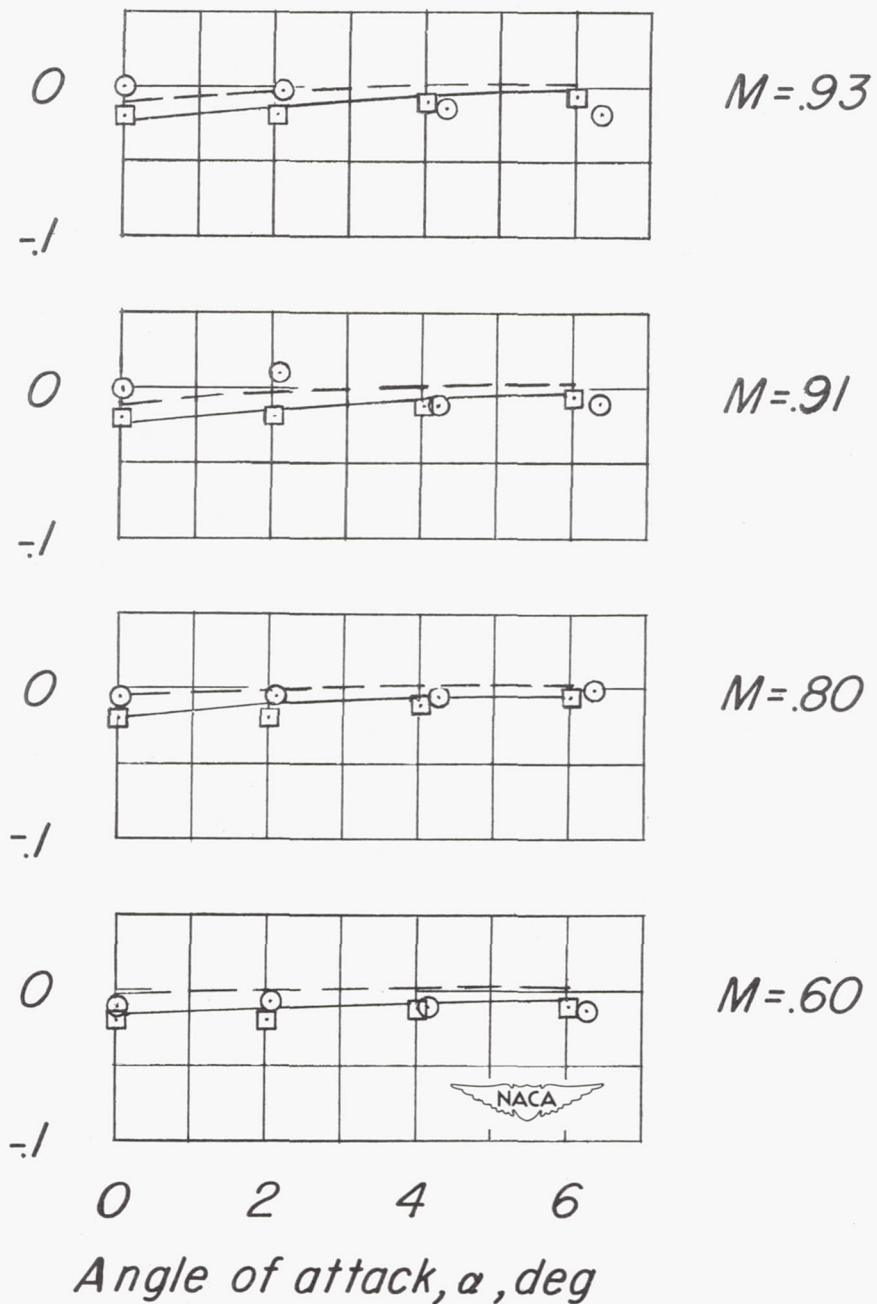
Figure 13.- Effect of the wing on the vertical-tail contribution to C_{l_p}.
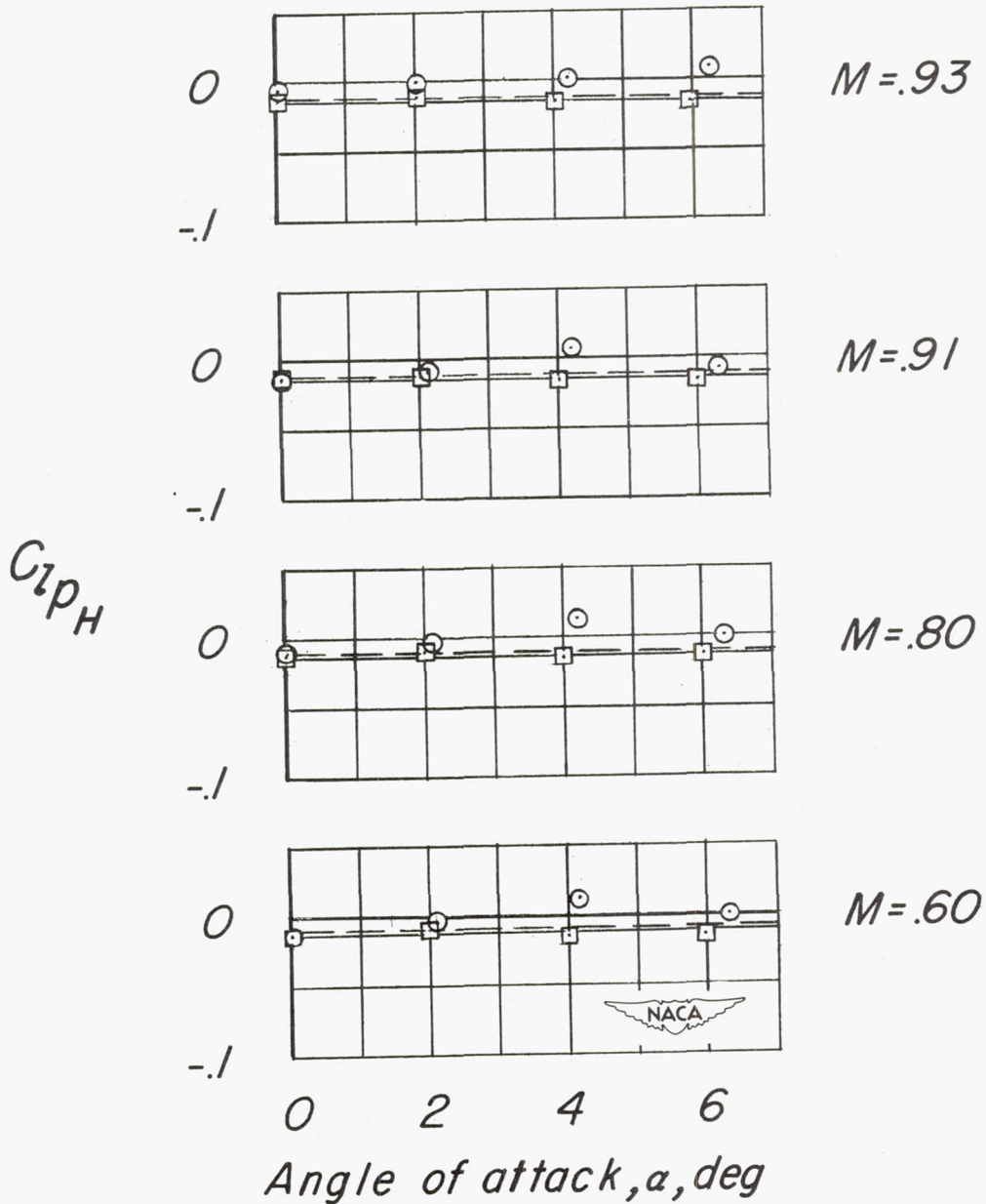
Figure 14.- Effect of the wing on the contribution of the horizontal tail to C_{l_p}.

○   *Experimental data(corrected for aeroelastic distortion)*

——   *Theory(figures 12,13,and 14)*
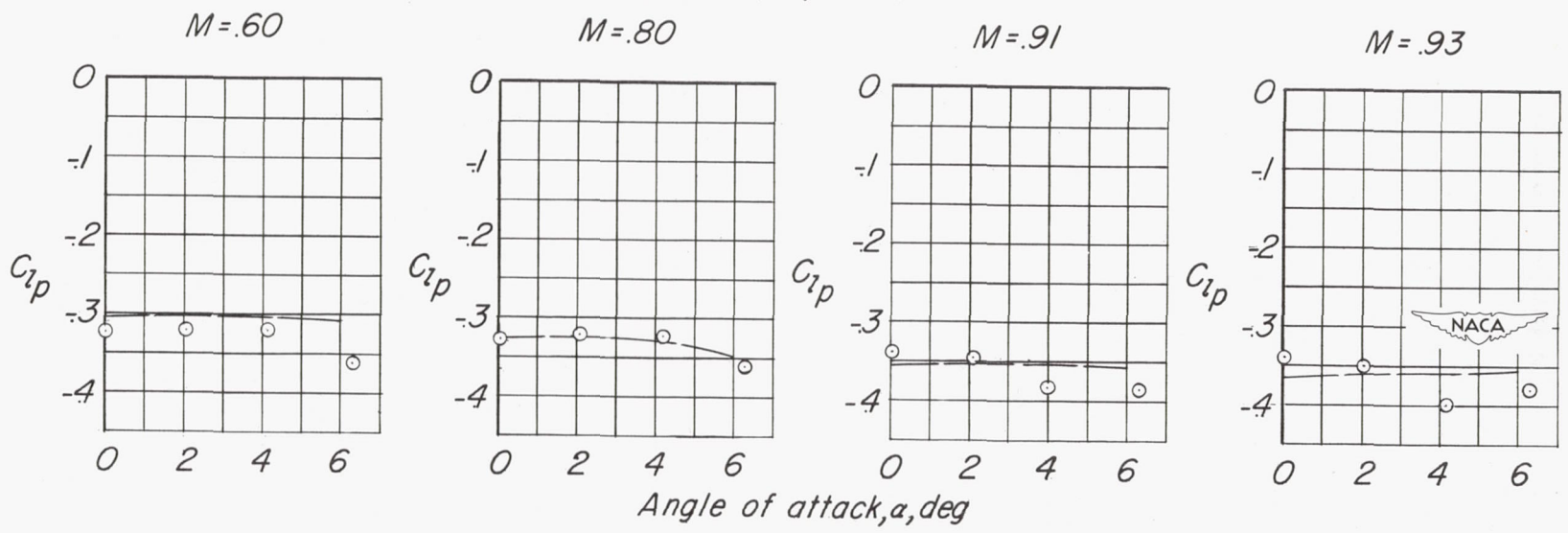
Figure 15.- Comparison of the experimental and theoretical damping-in-roll
coefficient for the complete model.
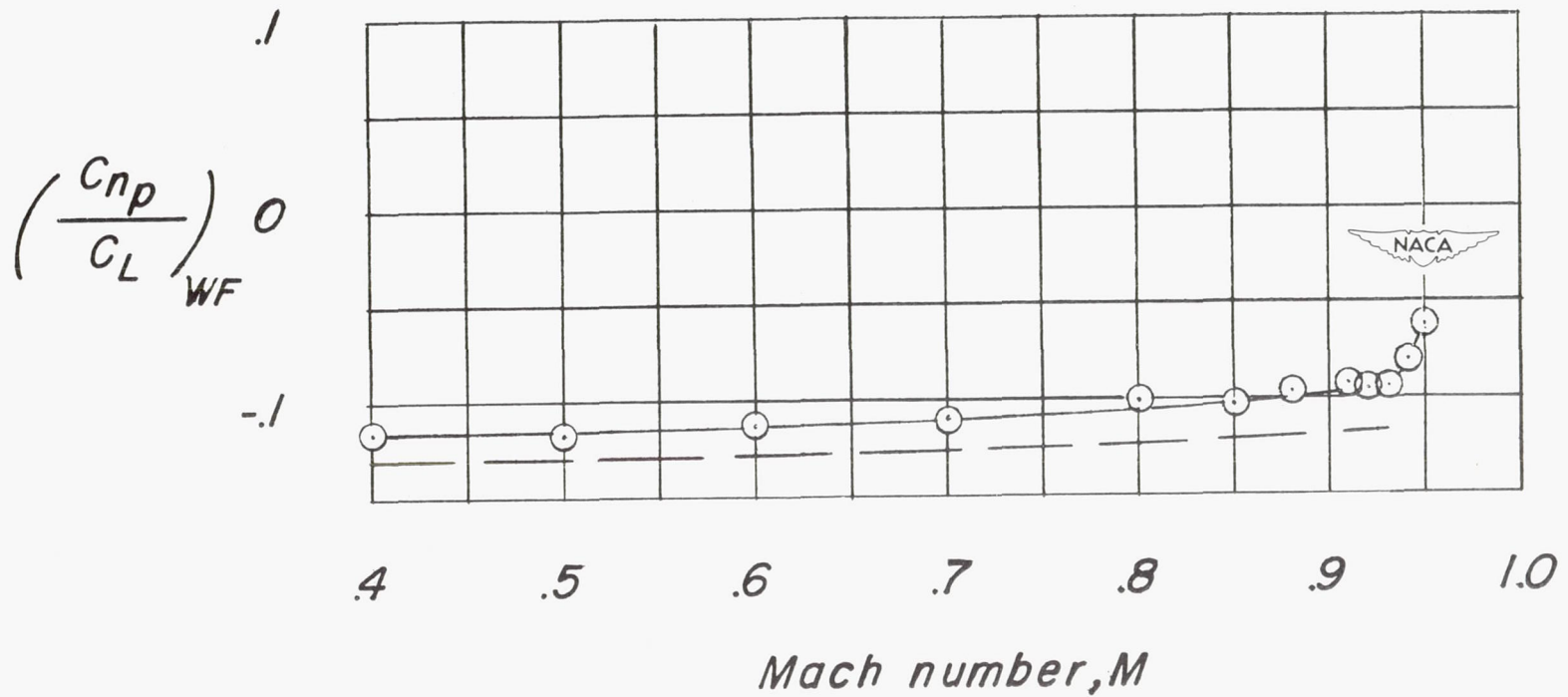
Figure 16.- Comparison of the experimental and theoretical variation of C_{n_p}/C_L with Mach number. $\alpha = 0^\circ$.

○ *Experimental data*

—— *Wing-alone theory (ref. 10)*

Cnp_{WF}
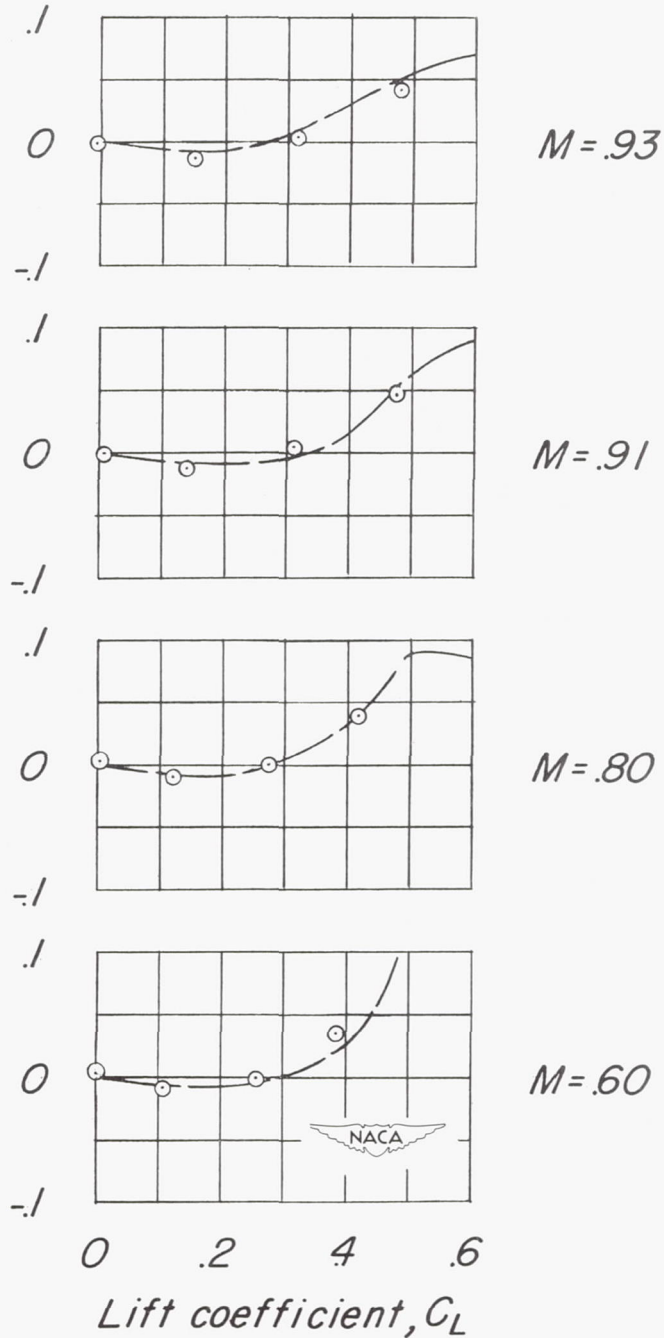
Figure 17.- Comparison of the theoretical and experimental variation of C_{n_p} with lift coefficient at several Mach numbers.
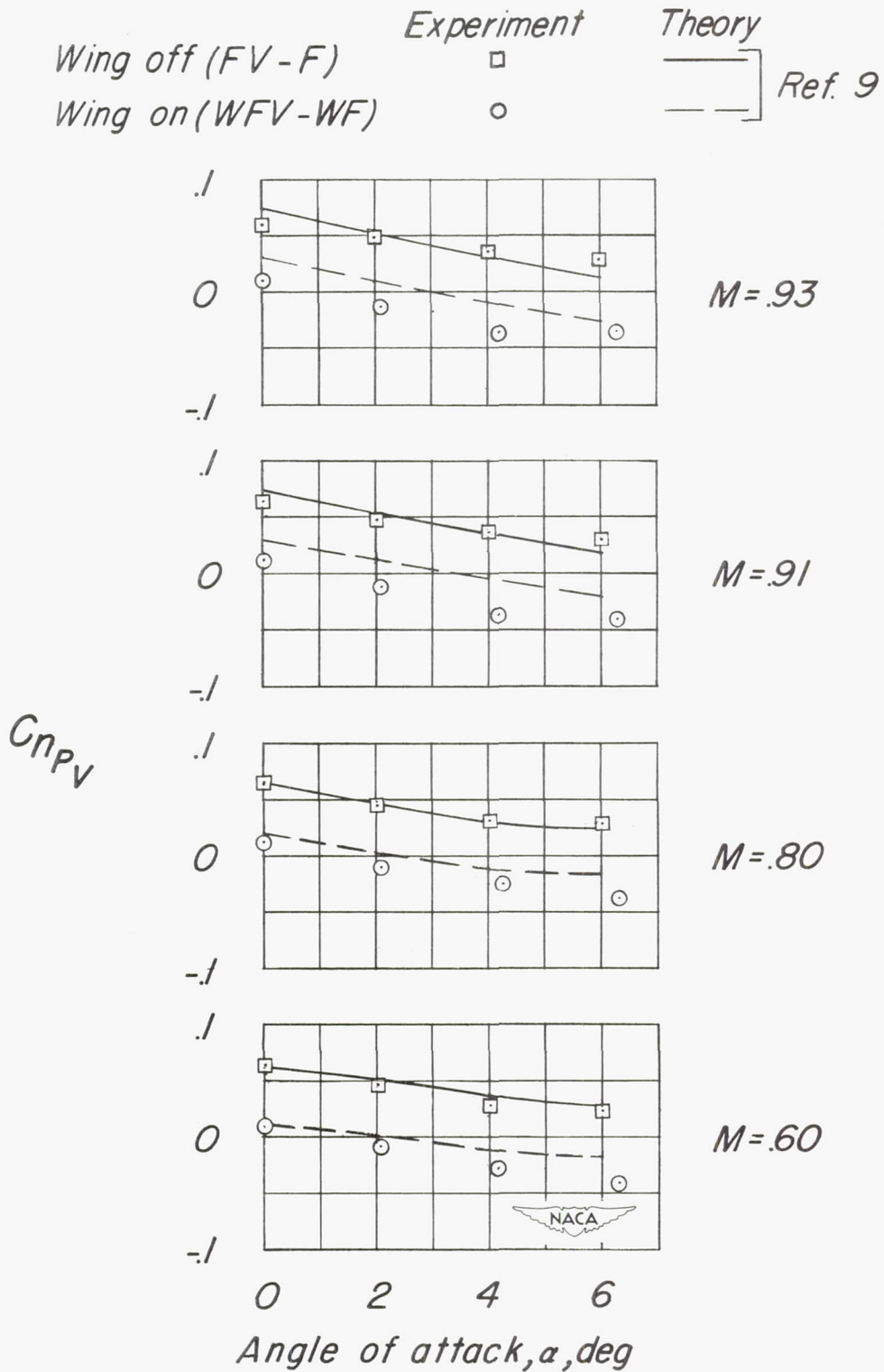
Figure 18.- Effect of the wing on the vertical-tail contribution to C_{n_p}.

Experiment

□ Wing off

○ Wing on
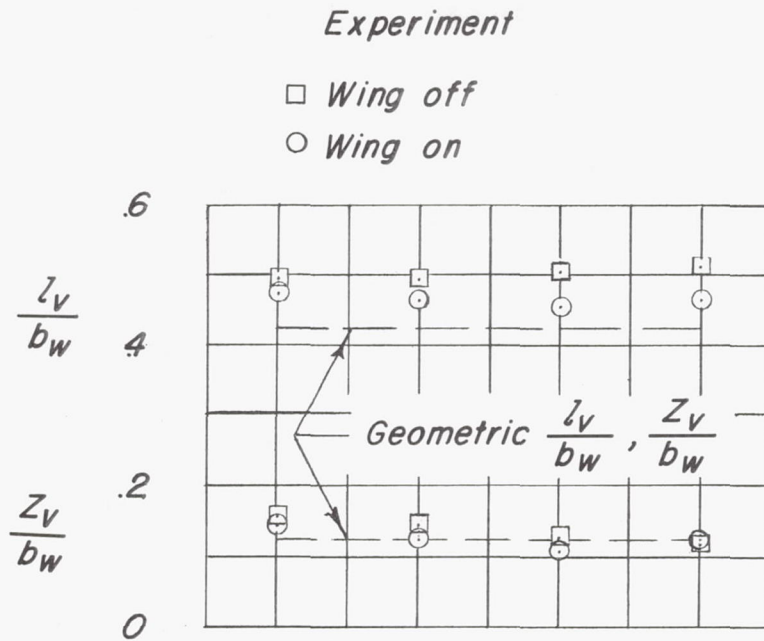
(a) Comparison of geometric and experimentally determined
tail centers of pressure.

Angle of attack, α, deg
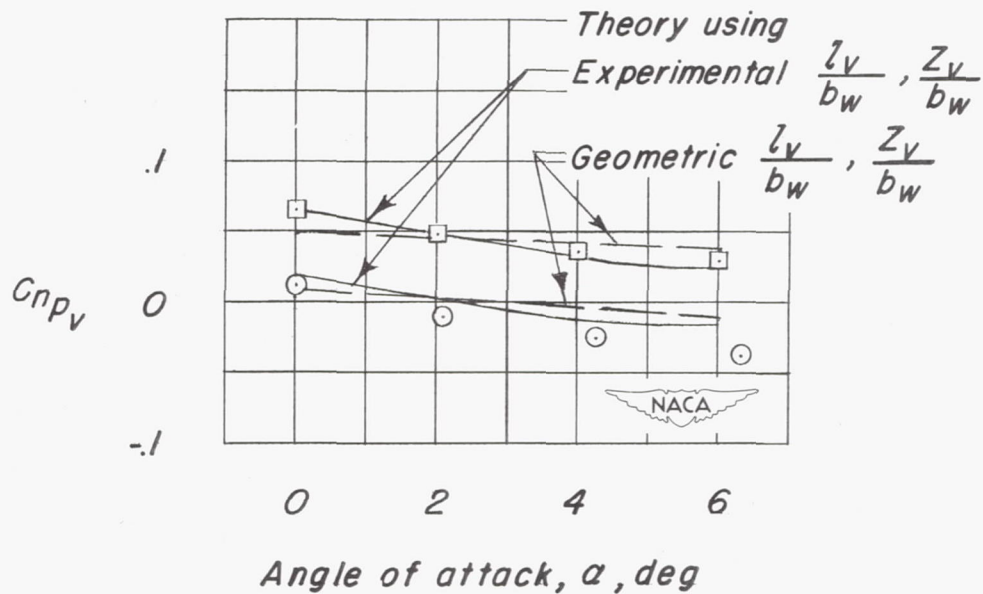
(b) Comparison of experimental and predicted values of $C_{n_{p_V}}$.

Figure 19.- Comparison of experimental values of $C_{n_{p_V}}$ with predictions

based on reference 9 in which tail centers of pressure are determined
either from simple geometry or from static lateral-stability data.
M = 0.80.
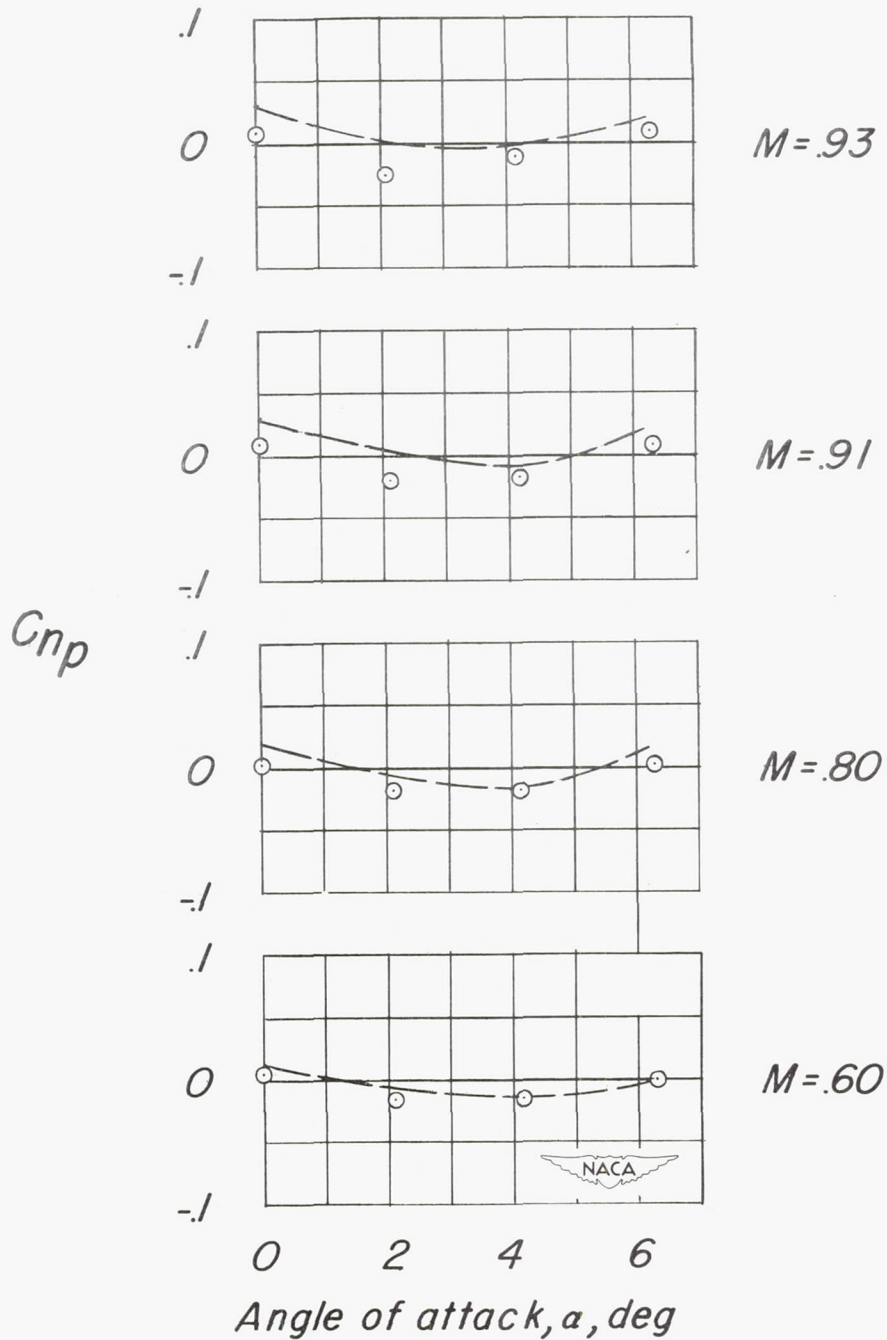
Figure 20.- Comparison of the experimental and theoretical values of C_{n_p} for the complete model.
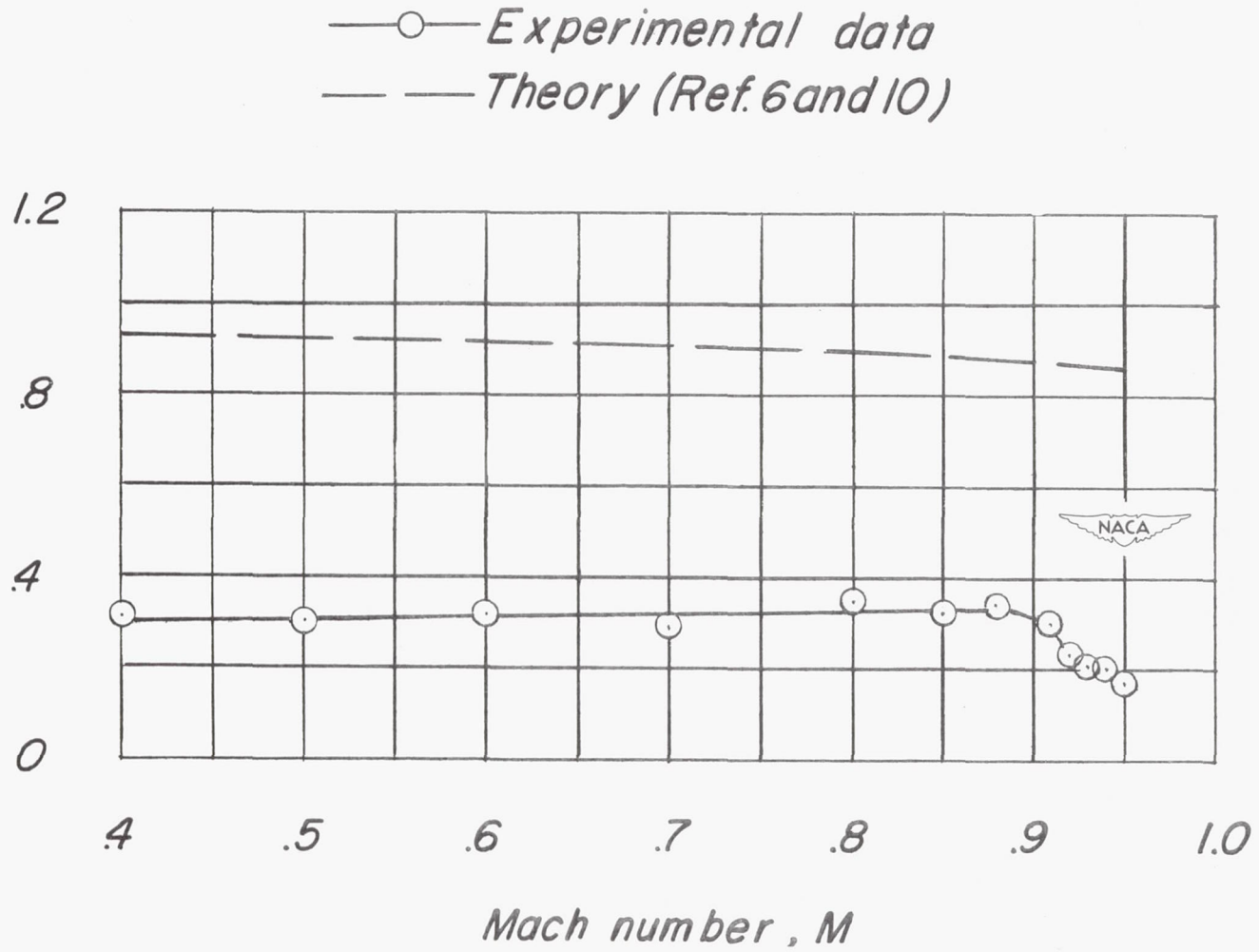
Figure 21.- Variation of C_{Y_p}/C_L with Mach number including a comparison with theory. $\alpha = 0°$.
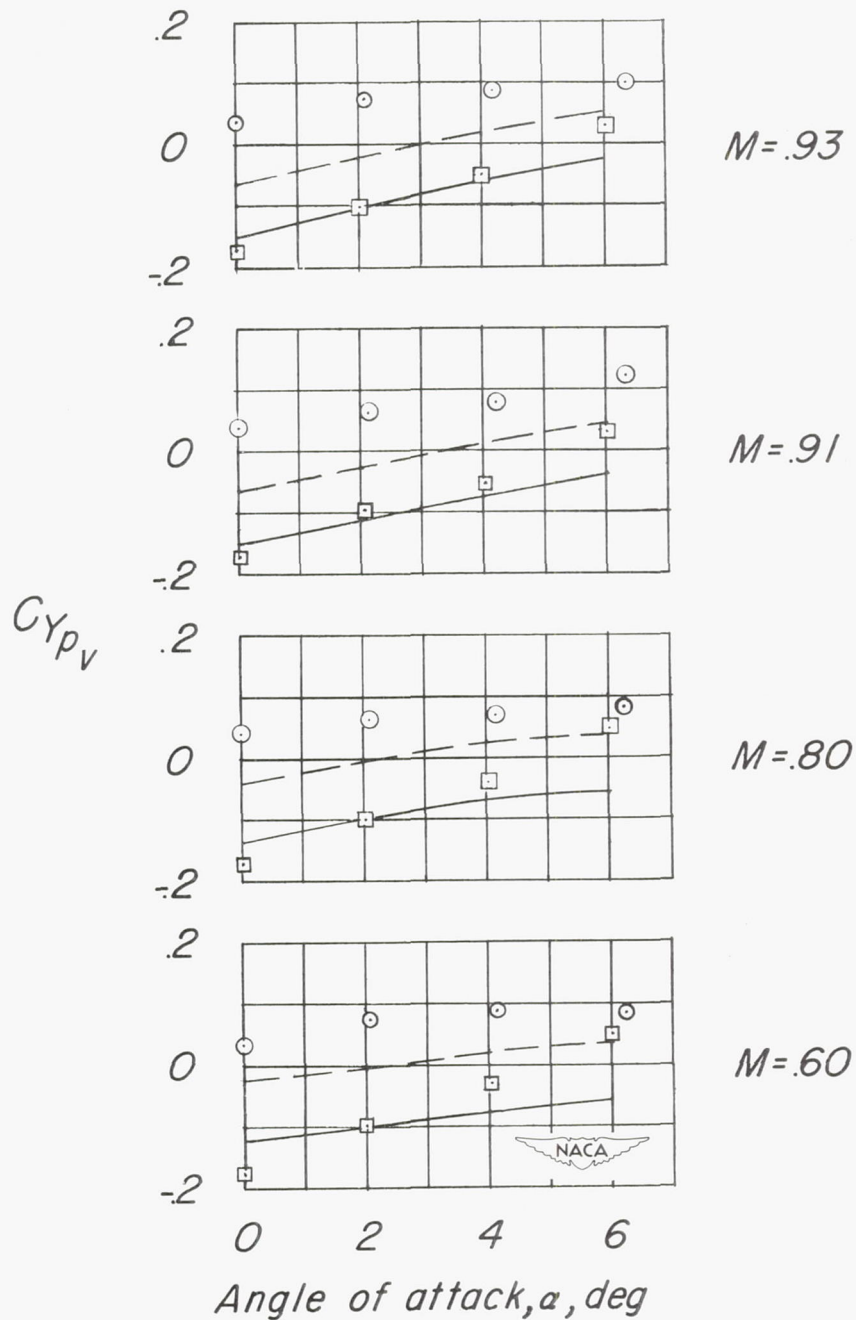
Figure 22.- Effect of the wing on the vertical-tail contribution to C_{Y_p}.
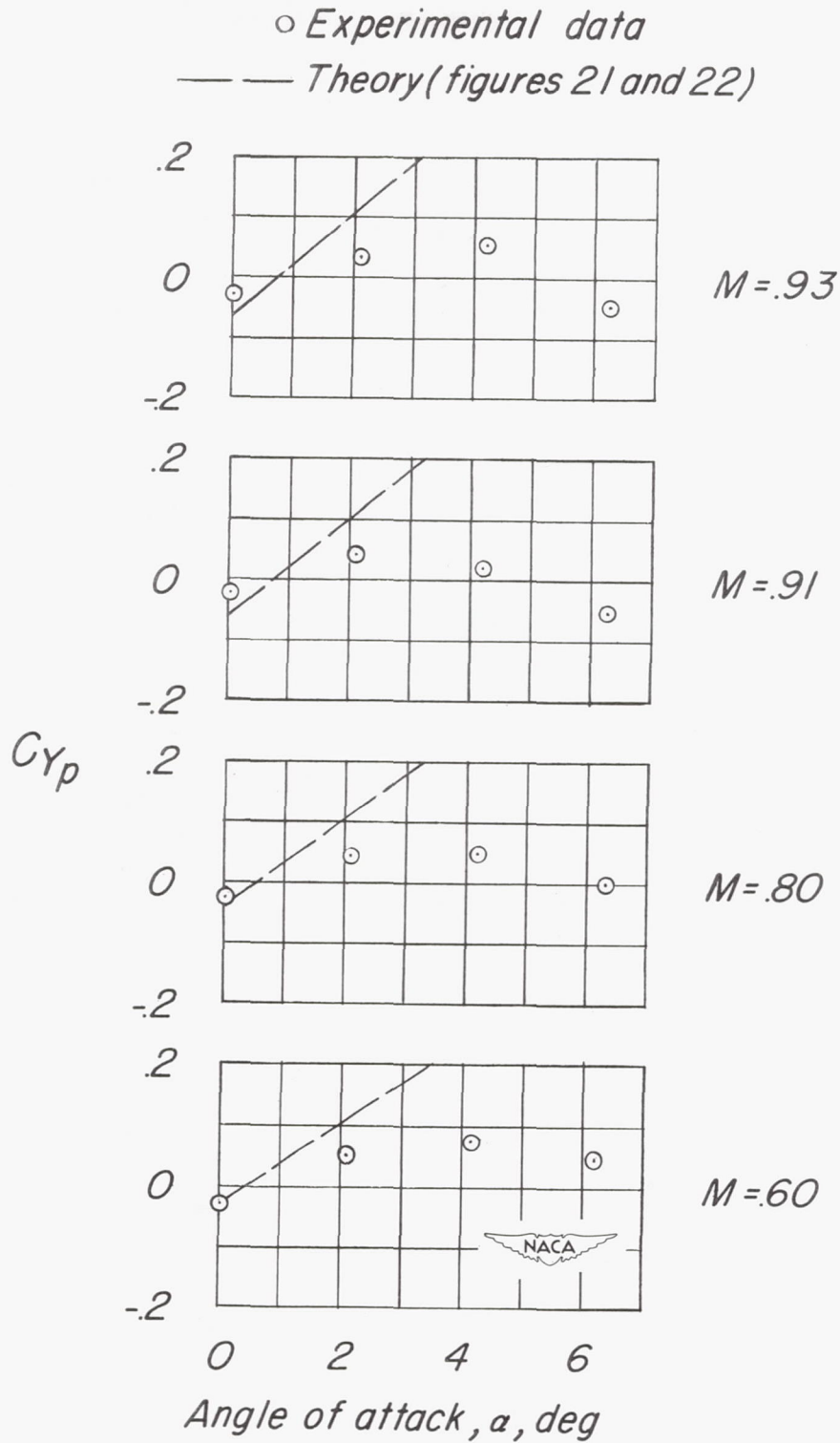
Figure 23.- Comparison of the experimental and theoretical values of C_{Y_p} for the complete model.